




# Quaking 5 suppresses TGF- $\beta$ -induced EMT and cell invasion in lung adenocarcinoma

Shengjie Wang<sup>1,2,3,†</sup> , Xin Tong<sup>1,2,†</sup>, Chang Li<sup>4,†</sup>, Ersuo Jin<sup>1,2</sup> , Zhiyue Su<sup>1,2</sup>, Zelong Sun<sup>1,2</sup>, Weiwei Zhang<sup>1,2</sup>, Zhe Lei<sup>1,2</sup> & Hong-Tao Zhang<sup>1,2,5,\*</sup> 

## Abstract

Quaking (QKI) proteins belong to the signal transduction and activation of RNA (STAR) family of RNA-binding proteins that have multiple functions in RNA biology. Here, we show that QKI-5 is dramatically decreased in metastatic lung adenocarcinoma (LUAD). QKI-5 overexpression inhibits TGF- $\beta$ -induced epithelial–mesenchymal transition (EMT) and invasion, whereas QKI-5 knockdown has the opposite effect. QKI-5 overexpression and silencing suppresses and promotes TGF- $\beta$ -stimulated metastasis *in vivo*, respectively. QKI-5 inhibits TGF- $\beta$ -induced EMT and invasion in a TGF $\beta$ 1-dependent manner. KLF6 knockdown increases TGF $\beta$ 1 expression and promotes TGF- $\beta$ -induced EMT, which is partly abrogated by QKI-5 overexpression. Mechanistically, QKI-5 directly interacts with the TGF $\beta$ 1 3' UTR and causes post-transcriptional degradation of TGF $\beta$ 1 mRNA, thereby inhibiting TGF- $\beta$ -induced SMAD3 phosphorylation and TGF- $\beta$ /SMAD signaling. QKI-5 is positively regulated by KLF6 at the transcriptional level. In LUAD tissues, KLF6 is lowly expressed and positively correlated with QKI-5 expression, while TGF $\beta$ 1 expression is up-regulated and inversely correlated with QKI-5 expression. We reveal a novel mechanism by which KLF6 transcriptionally regulates QKI-5 and suggest that targeting the KLF6/QKI-5/TGF $\beta$ 1 axis is a promising targeting strategy for metastatic LUAD.

**Keywords** KLF6; metastasis; QKI-5; TGF- $\beta$ -induced EMT; TGF $\beta$ 1

**Subject Categories** Cancer; RNA Biology; Signal Transduction

**DOI** 10.15252/embr.202052079 | Received 12 November 2020 | Revised 28

February 2021 | Accepted 8 March 2021 | Published online 26 March 2021

**EMBO Reports (2021) 22: e52079**

## Introduction

Improving clinical outcomes for lung cancer (LC) is still challenging due to its high metastasis and mortality (Jett *et al*, 1983; Siegel *et al*, 2019). Non-small-cell lung cancer (NSCLC) accounts for ~85% of

all LC cases, which includes lung adenocarcinoma (LUAD), lung squamous cell carcinoma (LUSC), and large cell carcinoma (Chen *et al*, 2014). LUAD represents the most common subtype of NSCLC and has the highest heterogeneity and aggressiveness (Kuhn *et al*, 2018). Thus, it is of great importance and urgency to elucidate the mechanisms underlying LUAD metastasis.

Epithelial–mesenchymal transition (EMT) has been demonstrated to associate with tumor initiation, metastasis, and drug resistance (Du & Shim, 2016; Pastushenko & Blanpain, 2019). When cells undergo EMT, epithelial markers (e.g., E-cadherin) are down-regulated while mesenchymal markers (e.g., N-cadherin and Snail) are up-regulated, accompanied by a cuboidal-to-spindle shape shift. These changes confer tumor cells with malignant characteristics, including increased metastatic capabilities (Dongre & Weinberg, 2019). Transforming growth factor- $\beta$  (TGF- $\beta$ )/SMAD signaling plays a predominant role in triggering EMT (Lamouille *et al*, 2014). Our previous studies indicated that activation of TGF- $\beta$ /SMAD signaling can drive TGF- $\beta$ -induced EMT in LUAD cells (Wang *et al*, 2016; Wang *et al*, 2018; Tong *et al*, 2020). TGF- $\beta$  receptor type I (TGF $\beta$ 1), an indispensable upstream receptor in TGF- $\beta$ /SMAD signal transduction, initiates a cascade reaction through phosphorylating R-SMADs and thereby activating the pathway (Schmierer & Hill, 2007). There is convincing evidence showing that dysregulation and dysfunction of TGF $\beta$ 1 can affect tumor metastasis by regulating TGF- $\beta$ /SMAD signaling in NSCLC and breast cancer (Fang *et al*, 2013; Wang *et al*, 2015; Kudinov *et al*, 2016).

Quaking (QKI) proteins, including three major isoforms QKI-5, QKI-6, and QKI-7, belong to the signal transduction and activation of RNA (STAR) family of RNA-binding proteins (RBPs). QKIs exert multiple functions in RNA biology, thereby affecting transcription, translation, shuttling between nucleus and cytoplasm, and non-coding RNA processing (Larocque *et al*, 2002; Wang *et al*, 2013; Zong *et al*, 2014; Conn *et al*, 2015; Zhou *et al*, 2017). Unlike QKI-6 and QKI-7 found in the cytoplasm, QKI-5 is mainly localized to the nucleus because it has a nuclear localization signal (Wu *et al*, 1999). It was reported that QKI-5 was frequently reduced in lung cancer (Zong *et al*, 2014; Zhou *et al*, 2017), suggesting a

1 Soochow University Laboratory of Cancer Molecular Genetics, Medical College of Soochow University, Suzhou, China

2 Department of Genetics, School of Biology and Basic Medical Sciences, Medical College of Soochow University, Suzhou, China

3 Department of Basic Medicine, Kangda College of Nanjing Medical University, Lianyungang, China

4 Department of Thoracic Surgery, The First Affiliated Hospital of Soochow University, Medical College of Soochow University, Suzhou, China

5 Suzhou Key Laboratory for Molecular Cancer Genetics, Suzhou, Jiangsu, China

\*Corresponding author. Tel: +86 512 65882809; E-mail: htzhang@suda.edu.cn

†These authors contributed equally to this work

tumor-suppressive role of QKI-5 in lung cancer. Most recently, Liang *et al* (2020) found that QKI-5 exhibited anticancer potential by inhibiting miR-196b-5p in NSCLC. To date, QKI-5 was identified to inhibit LUAD aggressiveness through preventing  $\beta$ -catenin activation (Zhou *et al*, 2017). However, an involvement of QKI-5 in TGF- $\beta$ /SMAD signaling and its underlying mechanisms remain unclear in LUAD. Moreover, the reason why QKI-5 is down-regulated in LUAD needs to be further elucidated.

Krüppel-like factor 6 (KLF6) is a broadly expressed zinc finger transcription factor, which has been found to be frequently decreased or inactivated in several human cancers, such as prostate cancer, colorectal cancer, and NSCLC (Narla *et al*, 2001; Ito *et al*, 2004; Reeves *et al*, 2004). Given that we have previously demonstrated that the transcriptional regulation of oncogenes or tumor suppressors participates in TGF- $\beta$ -induced EMT and NSCLC metastasis (Wang *et al*, 2016; Tong *et al*, 2020) and a series of computational algorithms predicted that two putative KLF6 binding sites (KBEs) are harbored in *QKI-5* gene promoter, it was proposed that KLF6 may transcriptionally regulate *QKI-5* during LUAD metastasis.

Here, we have screened for metastatic LUAD-associated RBPs and investigated whether QKI-5 contributes to TGF- $\beta$ -induced EMT and metastasis by regulating TGF- $\beta$ /SMAD signaling in LUADs. We have explored the novel mechanism by which KLF6 transcriptionally regulates *QKI-5* in LUADs and find that QKI-5 can prevent TGF- $\beta$ /SMAD signaling by post-transcriptionally inhibiting *TGF $\beta$ R1* mRNA and thereby repressing TGF- $\beta$ -induced EMT and metastasis of LUAD cells. Intriguingly, we also reveal that *QKI-5* is positively regulated by KLF6 at the transcriptional level. Our findings discover a KLF6/QKI-5/TGF $\beta$ R1 axis that blocks TGF- $\beta$ /SMAD signaling, providing new insight for a better understanding of TGF- $\beta$ -induced EMT and metastasis in LUAD.

## Results

### Identification of metastatic LUAD-associated QKI-5

In order to identify LUAD-associated RBPs, we firstly screened for the differentially expressed genes in 4 independent data sets, which meet the following criteria: (i) For TCGA\_LUAD database (<https://gdc.cancer.gov/>), false discovery rate (FDR) < 0.01 and the absolute value of  $\log_2$  fold change (abs. $\log_2$ FC) > 1 were applied; (ii) for lung cancer data sets of GSE40791, GSE75037, and GSE7670 from Gene Expression Omnibus (GEO) database (Chen *et al*, 2009; Zhang *et al*, 2012; Girard *et al*, 2016), adjusted *P*-value < 0.01 and abs. $\log_2$ FC > 1 were applied. Subsequently, ATtRACT database (Giudice *et al*, 2016) containing all human RBPs was intersected with the aforementioned four data sets to yield the differentially expressed RBPs. In total, we identified four differentially expressed RBPs associated with LUAD: ADARB1, CELF2, QKI, and ZFP36 (Fig 1A). Next, we detected the expression of these 4 LUAD-associated RBPs by qRT-PCR in 61 LUAD and matched paracarcinoma tissues, and LUAD tissues showed significant reduction in three RBPs (CELF2, QKI, and ZFP36) when compared with paracarcinoma tissues (Fig 1B upper panel and Appendix Table S1). However, we found that only *QKI* expression was significantly down-regulated in metastatic LUAD tissues (*n* = 28) compared with that in non-metastatic counterparts (*n* = 33), when 61 paired LUAD samples were divided into

metastatic and non-metastatic groups (Fig 1B lower panel and Appendix Table S1). Furthermore, clinical data analysis was performed to investigate the role of QKI in the progression and prognosis of LUAD. As a result, TCGA and CPTAC analysis (UALCAN, <http://ualcan.path.uab.edu/>) showed that *QKI* mRNA and protein levels were lower in LUAD tissues than those in normal lung tissues, and *QKI* expression was negatively correlated with the clinical stage of LUAD (Fig 1C and D). Kaplan–Meier survival analysis (<http://kmpplot.com/analysis/>) showed that low expression of *QKI* was significantly associated with poor survival in LUAD patients, but not in lung squamous carcinoma (LUSC; Fig 1E–G). Collectively, these data suggest that *QKI* is linked to LUAD metastasis.

In fact, *QKI* has three major isoforms, including *QKI-5*, *QKI-6*, and *QKI-7*. *QKI-5* is mainly localized in the nucleus due to its nuclear localization signal, while *QKI-6* and *QKI-7* are in the cytoplasm (Wu *et al*, 1999). In this study, *QKI-5* mRNA expression was far higher than *QKI-6* and *QKI-7* in LUAD cell lines A549 and H1299 (Fig 1H), and *QKI-5* mRNA and protein expression was significantly lower in A549 and H1299 cells than that in lung normal epithelial cell line BEAS-2B (Fig 1H and I). Moreover, the data regarding *QKI-5* can be reflected in LUAD tissues of patients (*n* = 61), which showed a significant reduction in *QKI-5* mRNA expression (47/61, 77.1%) when compared with matched paracarcinoma tissues (Fig 1J and K). Importantly, *QKI-5* mRNA expression was lower in metastatic LUAD tissues than that in non-metastatic counterparts (Fig 1L, Appendix Tables S2 and S3). Therefore, we will focus on *QKI-5* to explore the mechanisms behind its metastasis-suppressing potential in LUADs.

### QKI-5 directly interacts with *TGF $\beta$ R1* mRNA by targeting *TGF $\beta$ R1* 3' UTR in LUAD cells

Next, as shown in Fig 2A, we identified 2,511 potential *QKI*-targeted genes by integrating 3 RBP-binding sites database (POSTAR, EuRBPDB, and doRiNA) (Blin *et al*, 2015; Zhu *et al*, 2019; Liao *et al*, 2020). Interestingly, Kyoto Encyclopedia of Genes and Genomes (KEGG) enrichment analysis of these 2511 *QKI*-targeted genes revealed that 22 genes were part of the TGF- $\beta$  signaling pathway (Fig 2B). Among these 22 genes, *TGF $\beta$ R1*, an upstream receptor that initiates TGF- $\beta$ /SMAD signaling, has attracted our attention because we are interested in studying the crucial role of TGF- $\beta$  signaling in NSCLC metastasis (Wang *et al*, 2016; Wang *et al*, 2018; Tong *et al*, 2020). Thus, we performed nuclear/cytosol fractionation experiments and found that *QKI-5* was predominantly distributed in the nucleus (Fig 2C), being consistent with the previous report (Wu *et al*, 1999). Subsequently, we performed RIP using anti-*QKI-5* antibody and qRT-PCR assays in nuclear and cytoplasmic extracts from A549 and H1299 cells. The results indicated that *QKI-5* can specifically bind to *TGF $\beta$ R1* mRNA in the nucleus of A549 and H1299 cells (Fig 2D and E).

It has been well documented that *QKI* regulates gene expression by binding to 3' UTR of target mRNAs via a specific *QKI* response element [QRE, 5'-A(C/U)UAAAY] (Fig 2F) (Galarneau & Richard, 2005; Thangaraj *et al*, 2017). Sequence analysis revealed that there were two putative QREs at positions 2,108–2,113 and 2,486–2,491 in *TGF $\beta$ R1* 3' UTR, termed as QRE-1 and QRE-2 (Fig 2G upper panel). To verify whether the two predicted QREs affect the post-transcriptional regulation of *TGF $\beta$ R1* mRNA through interacting

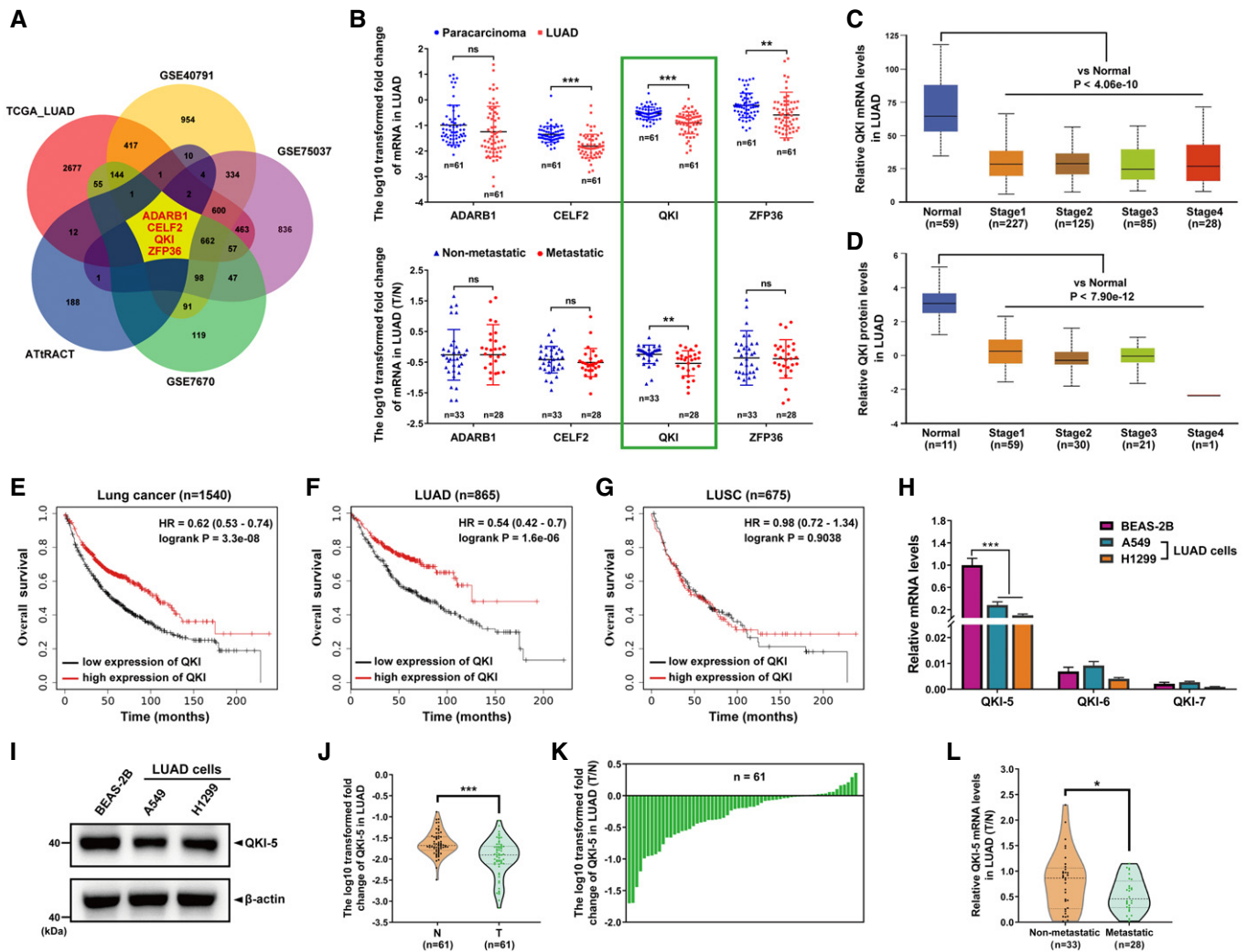


**Figure 1. Identification of metastasis-associated QKI in human LUAD.**

- A Four lung cancer data sets including TCGA\_LUAD database, and GSE40791, GSE75037, GSE7670 from GEO database were intersected with human RBP database ATTRACT to identify the differentially expressed RBPs in LUAD. The Venn diagram depicts the overlap between five independent data sets.
- B The upper panel showing qRT-PCR analysis of four identified LUAD-associated RBPs (ADARB1, CELF2, QKI, and ZFP36) mRNA levels in 61 LUAD tissues and matched paracarcinoma tissues. The lower panel showing relative mRNA expression (T/N) of the four RBPs in metastatic ( $n = 28$ ) and non-metastatic ( $n = 33$ ) LUAD tissues. LUAD tissues were classified into metastatic and non-metastatic tissues as described in Materials and Methods. T, LUAD tissues; N, paracarcinoma tissues. Y axis represents the  $\log_{10}$ -transformed fold change of mRNA expression (T/N) of four RBPs. Data are shown as the mean  $\pm$  SD. ns, not significant; \*\* $P < 0.01$  and \*\*\* $P < 0.001$  by unpaired Student's  $t$ -test.
- C, D Comparison of QKI mRNA and protein expression between normal lung tissues and LUAD tissues, which were stratified by clinical stages (Stages 1–4) in TCGA database. Data are shown as the boxplot. Central band: median; upper and lower line of boxes: upper and lower quartile; upper and lower line of whiskers: maximum and minimum.  $P < 0.001$  compared to normal lung tissues by unpaired Student's  $t$ -test.
- E–G Kaplan–Meier survival curves (<http://kmplot.com/analysis/>) of LC, LUAD, and LUSC patients ( $n = 1,540$ ,  $n = 865$ , and  $n = 675$ , respectively) with high or low expression levels of QKI. The log-rank test was used to analyze the difference between two groups.
- H qRT-PCR analysis of endogenous mRNA levels of *QKI-5*, *QKI-6*, and *QKI-7* in human bronchial epithelial cell line BEAS-2B, LUAD cell lines A549 and H1299. Data are shown as the mean  $\pm$  SD of  $n = 3$  technical replicates. \*\*\* $P < 0.001$  compared to BEAS-2B cells by unpaired Student's  $t$ -test.
- I Western blot analysis of QKI-5 protein levels in BEAS-2B, A549, and H1299 cells.  $\beta$ -actin was used as an internal control.
- J, K qRT-PCR analysis of *QKI-5* mRNA in 61 LUAD tissues and matched paracarcinoma tissues (J) and T/N mRNA expression of *QKI-5* in 61 paired LUAD tissues (K). T, LUAD tissues; N, paracarcinoma tissues. Y axis represents the  $\log_{10}$ -transformed fold change of mRNA expression of *QKI-5*. In the violin plot, central dotted line represents median, and upper and lower dotted line represents quartile (J). \*\*\* $P < 0.001$  by unpaired Student's  $t$ -test.
- L Violin plots showing *QKI-5* mRNA expression (T/N) in metastatic ( $n = 28$ ) and non-metastatic ( $n = 33$ ) LUAD tissues. Central dotted line of the violin plot represents median, and upper and lower dotted line represents quartile. \* $P < 0.05$  by unpaired Student's  $t$ -test.

Source data are available online for this figure.

with QKI-5, we prepared a series of *TGFβ1* 3' UTR fragments containing wild-type or mutant QRE-1/2 (Fig 2G lower panel and Appendix Table S4) and overexpressed QKI-5 via lentiviral

expression system in A549 and H1299 cells (Fig 2H). Then, we created various constructs encompassing above-mentioned *TGFβ1* 3' UTR fragments using Dual-Luciferase reporter vector (Fig 2I left

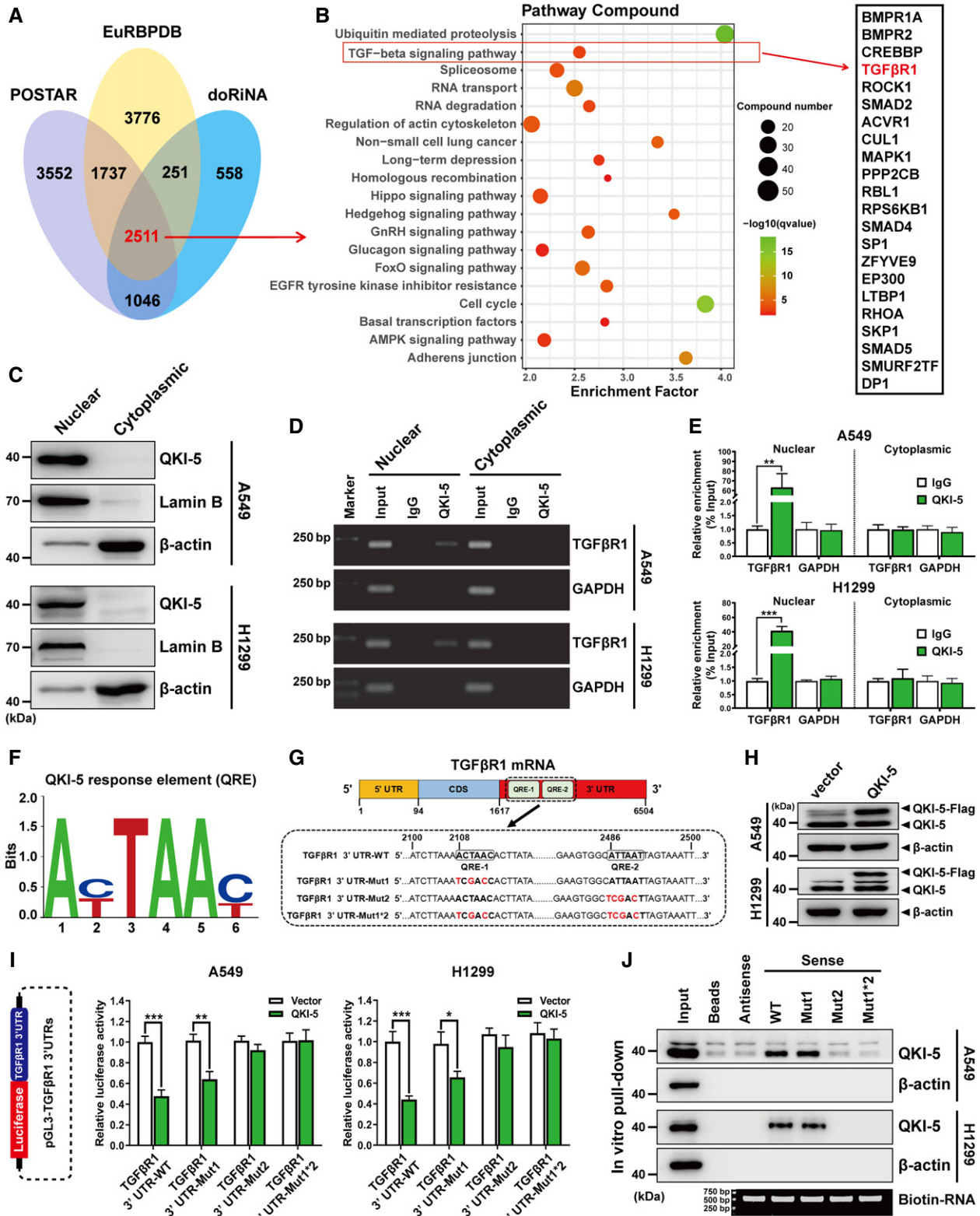


Figure 2.

**Figure 2. QKI-5 directly interacts with *TGFβ1* mRNA by targeting *TGFβ1* 3' UTR in LUAD cells.**

- A The Venn diagram depicts the identification of 2,511 QKI-targeted genes overlapping between three RBP-binding sites databases (POSTAR, EuRBPDB, and doRiNA).
- B KEGG enrichment analysis was performed by clusterProfiler in R language. Top 20 interested KEGG enrichment terms of 2,511 QKI-targeted genes identified in (A) were shown in left panel. A total of 22 genes were enriched in TGF-β signaling pathway, which were presented in right panel.
- C Western blot analysis of QKI-5 expression in nuclear and cytoplasmic fractions extracted from A549 and H1299 cells. Lamin B and β-actin were used as internal controls in nuclear and cytoplasmic extracts, respectively.
- D Anti-QKI-5 RIP was conducted in nuclear and cytoplasmic extracts from A549 cells and H1299 cells, and followed by RT-PCR and gel-staining analyses to examine *TGFβ1* mRNA enrichment. The input and anti-IgG antibody were used as positive and negative controls, respectively. *GAPDH* served as an internal RNA control in RT-PCR analysis.
- E After RIP assay, endogenous *TGFβ1* mRNA was enriched from A549 cells and H1299 cells and determined by qRT-PCR. Results were shown as the percentage of the enrichment to input. Data are shown as the mean ± SD of *n* = 3 technical replicates. \*\**P* < 0.01; \*\*\**P* < 0.001 by unpaired Student's *t*-test.
- F A conserved consensus QKI-5 response element (QRE) was presented.
- G Schematic drawing shows two predicted QREs in *TGFβ1* mRNA 3' UTR (upper panel). Boxed areas indicate several *TGFβ1* 3' UTR segments (positions, 2,058–2,557) containing wild type (*TGFβ1* 3' UTR-WT) or mutants of QRE-1/2 (*TGFβ1* 3' UTR-Mut1, *TGFβ1* 3' UTR-Mut2, and *TGFβ1* 3' UTR-Mut1\*2; lower panel), which are prepared to subclone into pGL3-Luc reporter vector. Numbers represent the nucleotide position of *TGFβ1* mRNA.
- H Western blot analyses of QKI-5 expressed in A549 and H1299 cells stably overexpressing Flag-tagged QKI-5.
- I Left panel: schematic drawing of the pGL3-*TGFβ1* 3' UTR luciferase reporter assay system. Middle and right panels: QKI-5-overexpressing and vector A549 and H1299 cells were transfected with pGL3-Luc reporter plasmids that were made by fusing the above-mentioned *TGFβ1* 3' UTR segments. Relative luciferase activities were determined as described in Materials and Methods and normalized to those in vector cells. Data are shown as the mean ± SD of *n* = 3 technical replicates. \**P* < 0.05, \*\**P* < 0.01 and \*\*\**P* < 0.001 by unpaired Student's *t*-test.
- J *In vitro* RNA pull-down assays were performed using biotin-labeled *TGFβ1* 3' UTR segments in A549 and H1299 cells. After pull-down, endogenous QKI-5 enrichments were detected by Western blot analyses. β-actin was used as the protein control.
- Source data are available online for this figure.

panel) and transfected them into A549 and H1299 cells overexpressing QKI-5. Luciferase reporter assay showed that QKI-5 overexpression resulted in a dramatic reduction in luciferase activity of *TGFβ1* 3' UTR. Importantly, we found that either the QRE-2 mutation or the combined mutations of QRE-1 and QRE-2, but not the QRE-1 mutation, abolished the inhibitory effects of QKI-5 overexpression on luciferase activity in A549 and H1299 cells (Fig 2I middle and right panels). To further confirm these luciferase data, we performed *in vitro* RNA pull-down assays in A549 and H1299 cells and detected that QKI-5 protein was obviously pulled down by biotin-labeled *TGFβ1* 3' UTR fragments carrying wild-type QRE-1/2 or mutant QRE-1 (Fig 2J), suggesting that QRE-2 of *TGFβ1* mRNA is a target site of QKI-5. Overall, these findings demonstrate that QKI-5 directly interacts with *TGFβ1* mRNA through binding to *TGFβ1* 3' UTR in LUAD cells.

**QKI-5 negatively regulates *TGFβ1* and TGF-β/SMAD signaling in LUAD cells**

Based on the aforementioned findings, we speculated that QKI-5 may post-transcriptionally regulate the expression of *TGFβ1* gene in LUAD cells. To test this, we performed qRT-PCR and Western blot assays to measure *TGFβ1* mRNA and protein levels in A549 and H1299 cells stably overexpressing or silencing QKI-5. We found that QKI-5 overexpression dramatically reduced the expression of *TGFβ1* at both mRNA and protein levels in A549 and H1299 cells (Fig 3A and B). On the contrary, knockdown of QKI-5 significantly increased the *TGFβ1* mRNA and protein expression in A549 and H1299 cells (Fig 3C and D). These data suggested that QKI-5 suppressed *TGFβ1* expression in LUAD cells. Accumulating evidence suggests that QKI plays critical and diverse biological roles in regulating RNA, including mRNA stability and translational efficiency (Saccomanno et al, 1999; Larocque et al, 2002; Wang et al, 2013; Zhou et al, 2017). In the present study, we conducted a standard mRNA stability assay (Rodrigues et al, 2016) to investigate whether QKI-5 affected the stability of *TGFβ1* mRNA. As expected,

upon actinomycin D treatment, *TGFβ1* mRNA expression was inhibited and decreased in time-dependent manner (Fig 3E and F). Importantly, *TGFβ1* mRNA reduction was significantly faster in QKI-5-overexpressing A549 and H1299 cells than that in control cells (Fig 3E), whereas the opposite tendency occurred in QKI-5-silenced A549 and H1299 cells (Fig 3F). In summary, these results indicate that QKI-5 promotes *TGFβ1* mRNA instability, supporting that QKI-5 is capable of accelerating *TGFβ1* mRNA degradation at post-transcriptional level in LUAD cells.

Given the fact that *TGFβ1* acts as an indispensable receptor in TGF-β/SMAD signal transduction (Schmierer & Hill, 2007), we are inspired to explore whether QKI-5 regulates TGF-β/SMAD signaling in LUAD cells. In addition, *TGFβ1* directly phosphorylates SMAD3, which is a hallmark of TGF-β/SMAD activation (ten Dijke & Hill, 2004). Therefore, we detected TGF-β-induced phosphorylation of SMAD3 (p-SMAD3) in QKI-5-overexpressing or QKI-5-silenced LUAD cells. Upon TGF-β1 stimulation, QKI-5 overexpression significantly inhibited the expression levels of p-SMAD3 under the precondition of not changing total SMAD3 protein levels in A549 and H1299 cells (Fig 3G and H). In contrast, shRNA-mediated silencing of QKI-5 enhanced the expression levels of p-SMAD3 in the presence of TGF-β1 (Fig 3I and J). Moreover, upon TGF-β1 stimulation, QKI-5-overexpressing A549 and H1299 cells showed significant changes in the expression of downstream genes of TGF-β/SMAD signaling, including PAI-1, Slug, Snail, E-cadherin, and/or N-cadherin (Fig 3K). Taken together, our results reveal that QKI-5 can negatively regulate *TGFβ1*, thereby undermining the TGF-β/SMAD signaling pathway in LUAD cells.

**QKI-5 represses TGF-β-induced EMT and migration and invasion of LUAD cells**

According to the above findings and our previous studies that TGF-β/SMAD activation promotes EMT and invasion of NSCLC cells (Wang et al, 2016; Tong et al, 2020), we hypothesized that QKI-5 may inhibit TGF-β-induced EMT and migration and invasion of



LUAD cells. Upon TGF- $\beta$ 1 stimulation, QKI-5-overexpressing A549 and H1299 cells exhibited significantly reduced protein levels of mesenchymal markers N-cadherin and Snail (Fig 4A). Moreover, we carried out IF assays using F-actin antibody to label the cytoskeleton of QKI-5-overexpressing LUAD cells with and without TGF- $\beta$ 1

treatment and examined cell morphology. After treatment with TGF- $\beta$ 1 for 24 h, A549 and H1299 cells expressing empty vector displayed the typical spindle-shape mesenchymal morphology, whereas A549 and H1299 cells overexpressing QKI-5 largely reversed the mesenchymal morphology (Fig 4B). Wound-healing

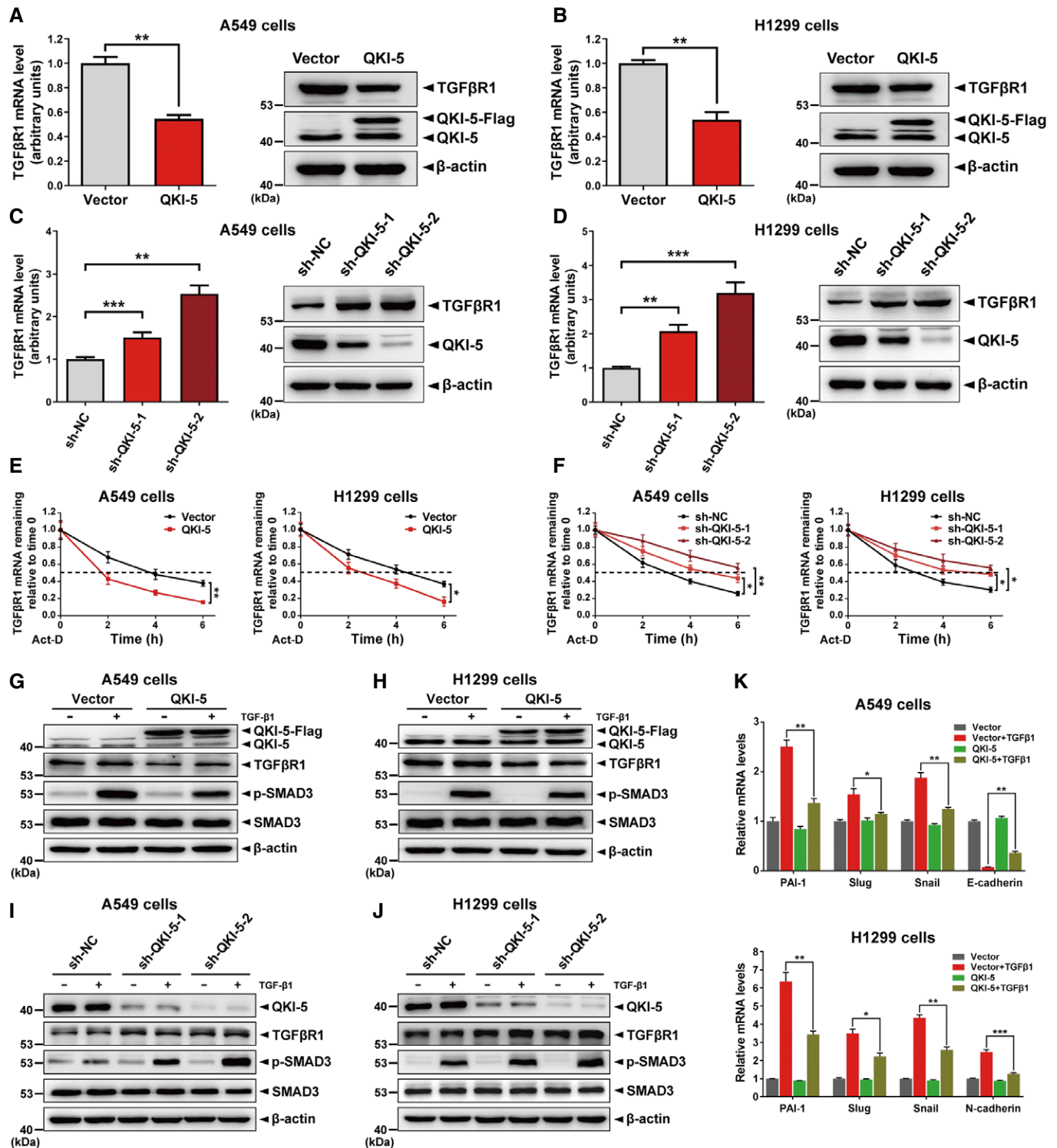


Figure 3.

**Figure 3. QKI-5 negatively regulates TGF $\beta$ R1 and TGF- $\beta$ /SMAD signaling in LUAD cells.**

- A, B qRT-PCR and Western blot analyses of TGF $\beta$ R1 mRNA and protein levels in QKI-5-overexpressing A549 and H1299 cells. Data are shown as the mean  $\pm$  SD of  $n = 3$  technical replicates. \*\* $P < 0.01$  by unpaired Student's  $t$ -test.
- C, D Expression of TGF $\beta$ R1 mRNA and protein in QKI-5-silenced A549 and H1299 cells. \*\* $P < 0.01$  and \*\*\* $P < 0.001$  by unpaired Student's  $t$ -test.
- E, F The mRNA stability of TGF $\beta$ R1 was examined in QKI-5-overexpressing/-silenced and control A549 and H1299 cells. Cells were treated with actinomycin D (Act-D, 10  $\mu$ g/ml) for 0, 2, 4, or 6 h, and mRNA levels of TGF $\beta$ R1 were determined by qRT-PCR. The quantity value of qRT-PCR at 0 h was set 1. \* $P < 0.05$  and \*\* $P < 0.01$  by unpaired Student's  $t$ -test.
- G, H After being serum-starved for 24 h, A549 and H1299 cells stably overexpressing QKI-5 were treated with or without TGF- $\beta$ 1 (5 or 10 ng/ml) for 24 h and subjected to Western blot assays to determine the protein levels of QKI-5, TGF $\beta$ R1, p-SMAD3, and SMAD3.  $\beta$ -actin was used as an internal control.
- I, J QKI-5-silenced A549 and H1299 cells were treated as above. Then, Western blot analysis was conducted to examine the protein levels of QKI-5, TGF $\beta$ R1, p-SMAD3, and SMAD3.
- K QKI-5-overexpressing A549 and H1299 cells were treated as above and subjected to qRT-PCR assays to detect the mRNA expression of downstream genes of the TGF- $\beta$ /SMAD signaling, including *PAI-1*, *Slug*, *Snail*, *E-cadherin*, and/or *N-cadherin*. Data are shown as the mean  $\pm$  SD of  $n = 3$  technical replicates. \* $P < 0.05$ , \*\* $P < 0.01$  and \*\*\* $P < 0.001$  by unpaired Student's  $t$ -test.

Source data are available online for this figure.

migration assay, as well as Transwell migration and invasion assays, showed that QKI-5 overexpression significantly suppressed TGF- $\beta$ -induced migratory and invasive capabilities of A549 and H1299 cells (Fig 4C–J). Furthermore, shRNA-mediated silencing of QKI-5 effectively promoted TGF- $\beta$ -induced EMT by downregulating E-cadherin or upregulating N-cadherin and Snail in A549 and H1299 cells (Fig EV1A–D) and enhanced TGF- $\beta$ -induced migratory and invasive abilities (Fig EV1E–H). Collectively, these results show that QKI-5 inhibits TGF- $\beta$ -induced EMT and migration and invasion of LUAD cells.

**QKI-5 attenuates TGF- $\beta$ -stimulated LUAD cell metastasis *in vivo***

To further elucidate the function of QKI-5 exerting in LUAD cell metastasis *in vivo*, we injected BALB/c nude mice intravenously (i.v.) with A549 cells stably overexpressing QKI-5 and vector control A549 cells, followed by injecting intraperitoneally (i.p.) with TGF- $\beta$ 1, established an *in vivo* model of LUAD metastasis (Fig 5A and B). At eight weeks post-inoculation, the mice were euthanized and their lungs and livers were surgically resected for evaluation of metastases and histology (Fig 5A). As shown in Fig 5C and D, the mice injected with QKI-5-overexpressing A549 cells developed fewer metastatic lung nodules than those injected with control A549 cells. The metastatic liver nodules were macroscopically undetectable in mice. However, the results of hematoxylin-eosin (H&E) staining showed that the injection of QKI-5-overexpressing A549 cells resulted in significantly fewer micro-metastatic foci in lung and liver tissues as compared with vector control group (Fig 5E–H). Moreover, the mice injected with QKI-5-silenced A549 cells exhibited more metastatic lung nodules and micrometastatic foci than those injected with control cells (Fig 5E–K). Taken together, the *in vivo* metastasis assays show that QKI-5 suppresses TGF- $\beta$ -stimulated metastasis of LUAD cells, further supporting our *in vitro* findings.

**Knockdown of TGF $\beta$ R1 suppresses TGF- $\beta$ -induced EMT and invasion of LUAD cells**

Since QKI-5 overexpression effectively reduced TGF $\beta$ R1 expression (Fig 3A and B) and repressed TGF- $\beta$ -induced EMT and LUAD cell metastasis *in vitro* and *in vivo* (Figs 4A–J and 5C–H), we next explored whether TGF $\beta$ R1 silencing could copy the phenotype

caused by QKI-5 overexpression. As illustrated in Fig EV2A–D, shRNA-mediated silencing of TGF $\beta$ R1 decreased the expression levels of p-SMAD3 and mesenchymal markers N-cadherin and Snail in A549 and H1299 treated with TGF- $\beta$ 1. Furthermore, Transwell assays indicated that TGF $\beta$ R1 silencing markedly inhibited TGF- $\beta$ -induced migratory and invasive capabilities of A549 and H1299 cells (Fig EV2E–H). Taken together, our results show that TGF $\beta$ R1 silencing can block TGF- $\beta$ /SMAD signaling and inhibit TGF- $\beta$ -induced EMT and invasion of LUAD cells, which mimics the phenotypic changes resulted from QKI-5 overexpression in LUADs.

**QKI-5 inhibits TGF- $\beta$ -induced EMT and cell invasion via a TGF $\beta$ R1-dependent manner**

Our aforementioned results indicate that QKI-5 not only represses TGF $\beta$ R1, but also inhibits TGF- $\beta$ -induced EMT and invasion in LUAD cells. To address the question of whether QKI-5 regulates these biological processes in a TGF $\beta$ R1-dependent manner, we first performed a direct rescue experiment in A549 and H1299 cells overexpressing QKI-5 and TGF $\beta$ R1 ORF-only. TGF $\beta$ R1 cDNA, lacks the 3'UTR containing QREs, not only restored the TGF $\beta$ R1 expression repressed by QKI-5 overexpression in A549 and H1299 cells (Fig 6A) but also abolished the inhibition of p-SMAD3, N-cadherin, and Snail caused by QKI-5 overexpression in A549 and H1299 cells treated with TGF- $\beta$ 1 (Fig 6B). Importantly, the TGF $\beta$ R1 cDNA overexpression rescued TGF- $\beta$ -induced migratory and invasive capabilities of A549 and H1299 cells overexpressing QKI-5 in the presence of TGF- $\beta$ 1 (Fig 6C–F). Moreover, TGF $\beta$ R1 mRNA expression was significantly up-regulated (51/61, 83.6%) in 61 LUAD tissues (Fig 6G and H) and negatively correlated with QKI-5 mRNA expression (Figs 6I and 1K). Importantly, TGF $\beta$ R1 mRNA expression was higher in metastatic LUAD tissues than that in non-metastatic counterparts (Appendix Tables S2 and S3). Kaplan–Meier survival analysis (<http://kmpplot.com/analysis/>) showed that LUAD patients with high expression of TGF $\beta$ R1 had a significantly poor survival (Fig 6J).

Furthermore, we treated A549 cells with SB431542, a specific TGF $\beta$ R1 kinase inhibitor (Mikami *et al*, 2006; Muppala *et al*, 2017), blocked TGF- $\beta$ /SMAD signaling. Being consistent with the impact of QKI-5 overexpression on cell invasion, SB431542 abolished TGF- $\beta$ -mediated migratory and invasive abilities of A549 cells (Fig EV3A

and B), indicating that the invasion-suppressing action of QKI-5 overexpression was recapitulated by TGF $\beta$ R1 inhibitor. SB431542 almost completely offset the promotion effect of QKI-5 silencing on

TGF- $\beta$ -induced migratory and invasive abilities of A549 cells (Fig EV3C and D), suggesting that TGF $\beta$ R1 inhibitor abolished the effects of QKI-5 silencing on TGF- $\beta$ -induced cell invasion. Taken together,

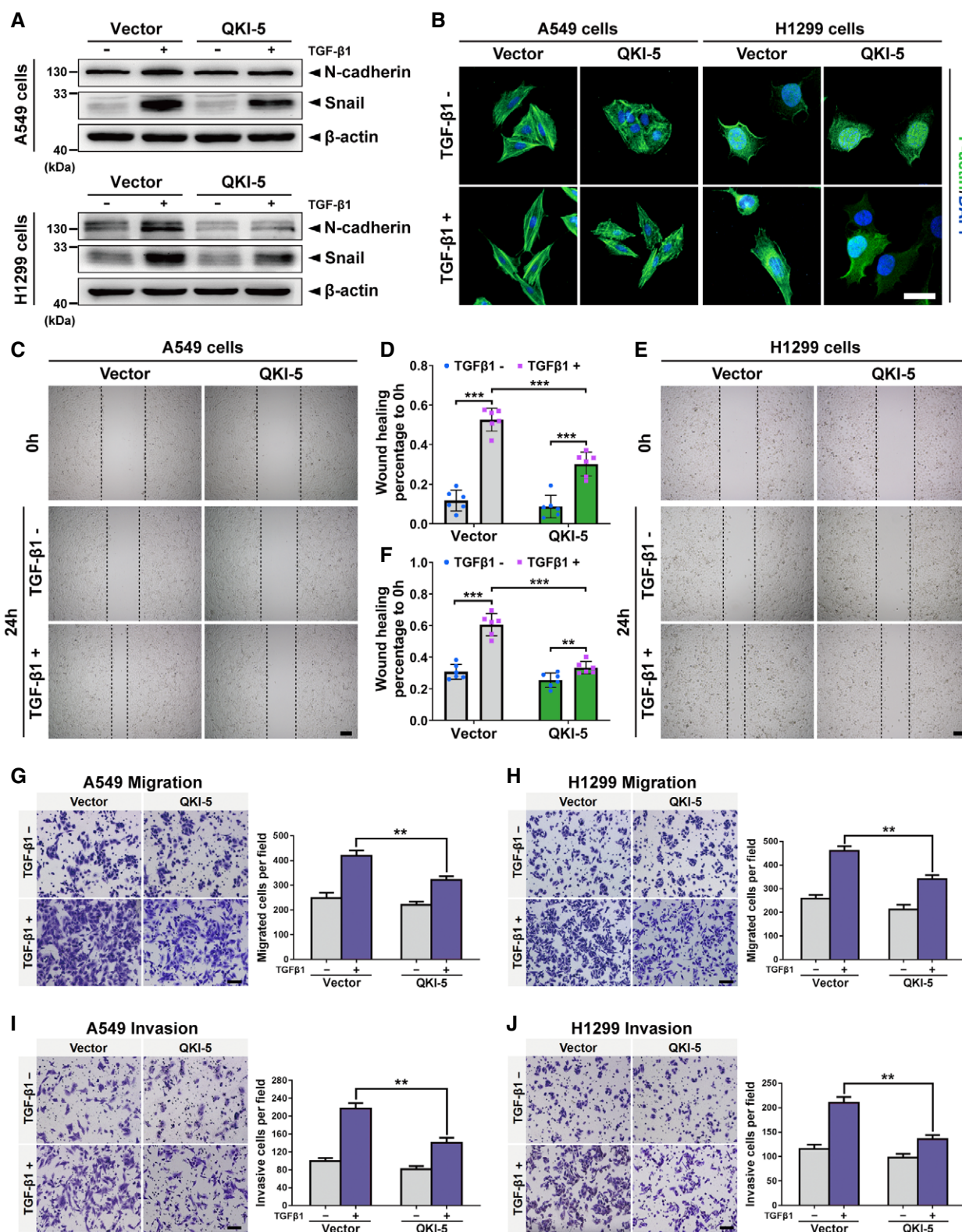


Figure 4.



**Figure 4. QKI-5 overexpression inhibits TGF- $\beta$ -induced EMT and migration and invasion of LUAD cells.**

- A After serum starvation for 24 h, A549 and H1299 cells overexpressing QKI-5 were treated with or without TGF- $\beta$ 1 (5 or 10 ng/ml) for 24 h. Then, EMT markers N-cadherin and Snail expression were analyzed using Western blot.  $\beta$ -actin served as an internal control.
- B QKI-5-overexpressing A549 and H1299 cells and control cells were treated as above and incubated with a mouse anti-F-actin antibody and then stained with a FITC-conjugated anti-mouse IgG (green, for F-actin). Cell nuclei were counterstained and visualized with DAPI (blue). Scale bar, 100  $\mu$ m.
- C–F Wound-healing migration assays were performed on QKI-5-overexpressing A549 and H1299 cells as well as control cells, which were treated as above. The wound healing was recorded (C, E) and quantitatively measured (D, F) at least six times. Data are shown as the mean  $\pm$  SD of  $n = 6$  technical replicates. \*\* $P < 0.01$  and \*\*\* $P < 0.001$  by unpaired Student's  $t$ -test. Scale bar, 100  $\mu$ m.
- G, H In the presence or absence of TGF- $\beta$ 1, QKI-5-overexpressing A549 and H1299 cells were allowed to migrate through a polycarbonate membrane in Transwells. After 24 h, migrated cells were stained, photographed, and counted in at least four random fields under a light microscope. Representative images (left) and the migrated cell numbers (right) were presented. Data are shown as the mean  $\pm$  SD of  $n = 3$  technical replicates. \*\* $P < 0.01$  by unpaired Student's  $t$ -test. Scale bar, 100  $\mu$ m.
- I, J QKI-5-overexpressing A549 and H1299 cells were treated as above and allowed to invade through Matrigel-coated membrane in Transwells. Invasive cells were determined as described above. Scale bar, 100  $\mu$ m. Data are shown as the mean  $\pm$  SD of  $n = 3$  technical replicates. \*\* $P < 0.01$  by unpaired Student's  $t$ -test.

Source data are available online for this figure.

our results demonstrate that QKI-5 inhibits TGF- $\beta$ -induced EMT, LUAD cell migration, and invasion in a TGF $\beta$ R1-dependent manner.

**KLF6 transcriptionally regulates QKI-5 gene in LUADs**

Subsequently, we explored why *QKI-5* was frequently down-regulated in LUADs. First, after intersecting the aforementioned four data sets (Fig 1A) with human TFs database JASPAR (Fornes *et al*, 2020), we obtained 25 differentially expressed TFs in LUADs, 10 of which were predicted to have potential binding sites in the *QKI-5* promoter (Fig 7A and B). Of note, knockdown of FLI1, KLF6, and TBX3 expression (Fig 7C) significantly affected *QKI-5* mRNA expression in A549 cells (Fig 7D). In this study, more attention was paid to KLF6 because of it was frequently reduced in various human cancers, including NSCLC (Narla *et al*, 2001; Ito *et al*, 2004; Reeves *et al*, 2004). Furthermore, we found that KLF6 knockdown also attenuated QKI-5 protein levels in A549 cells (Fig 7E). These results suggested that KLF6 may positively regulate *QKI-5* at transcriptional level. By analyzing KLF6-ChIP-seq data (GSE96355), we found an obvious peak (position  $-100$  to  $+100$ ) flanking the *QKI-5* promoter (Fig 7F). Also, we predicted two putative KLF6-binding elements (KBEs) at positions  $-346$  to  $-336$  (termed as KBE1) and  $+21$  to  $+31$  (termed as KBE2) in *QKI-5* promoter (QP) using PROMO and JASPAR (Fig 7G upper panel). Subsequently, ChIP assays in A549 cells showed that a DNA fragment containing KBE2 rather than KBE1 in  $\Delta$ QP was enriched using anti-KLF6 antibody (Fig 7G lower panel), indicating a direct interaction of KLF6 with *QKI-5* promoter via binding to KBE2.

Next, to clarify whether KLF6 contributes to *QKI-5* transcriptional activity through KBE2, we constructed four different pGL3- $\Delta$ QP luciferase reporter plasmids containing wild type or mutants of KBE1 and 2 (Fig 7H left panel and Appendix Table S4) and co-transfected them with *KLF6* siRNAs into A549 cells. Results of luciferase reporter assay showed that pGL3- $\Delta$ QP activity inhibition by KLF6 knockdown was abolished only when KBE2 was mutated (Fig 7H right panel), indicating that KBE2 of *QKI-5* promoter is a functional KLF6-binding site. In support of these results, *KLF6* mRNA expression was significantly down-regulated (46/61, 75.4%) in 61 LUAD tissues (Fig 7I and J) and positively correlated with *QKI-5* mRNA expression (Figs 7K and 1K). Taken together, these results reveal a transcriptional regulation mechanism of *QKI-5* by KLF6, being responsible for the altered expression of *QKI-5* in LUADs.

**KLF6 knockdown leads to an increase in TGF $\beta$ R1 expression and promotes TGF- $\beta$ -induced EMT and LUAD cell invasion, which is mediated by QKI-5**

Based on the aforementioned findings that QKI-5 repressed TGF $\beta$ R1 expression (Fig 3A and B) and inhibited TGF- $\beta$ -induced EMT and invasion of LUAD cells (Fig 4A–J) while KLF6 positively regulated *QKI-5* expression at transcriptional level (Fig 7C–H), we were encouraged to investigate whether KLF6 reduces TGF $\beta$ R1 expression and inhibits TGF- $\beta$ -induced EMT in a QKI-5-dependent manner. Firstly, a rescue experiment combining KLF6 knockdown and QKI-5 overexpression was performed to determine the expression of TGF $\beta$ R1 and EMT markers. As a result, siRNA-mediated knockdown of KLF6 caused a robust increase in mRNA and protein levels of TGF $\beta$ R1, which was significantly abrogated by QKI-5 overexpression in A549 cells (Fig EV4A and B). Moreover, knockdown of KLF6 increased the expression levels of p-SMAD3 and mesenchymal markers N-cadherin and Snail in A549 cells treated with TGF- $\beta$ 1. However, QKI-5 overexpression partly abolished the increase of p-SMAD3, N-cadherin, and Snail expression caused by KLF6 knockdown (Fig EV4C). Furthermore, wound-healing and Transwell assays showed that knockdown of KLF6 markedly prompted TGF- $\beta$ -induced migratory and invasive capabilities of A549 cells, whereas this promotion effect was significantly impaired by QKI-5 overexpression (Fig EV4D–G). Collectively, these results indicate KLF6 regulates TGF $\beta$ R1 expression and TGF- $\beta$ -induced EMT as well as LUAD cell invasion, which were largely mediated by QKI-5.

**Discussion**

So far, whether and how RBPs regulates TGF- $\beta$ /SMAD signaling and act on TGF- $\beta$ -induced EMT and metastasis of LUAD cells remains poorly understood. In this study, we identified a metastatic LUAD-associated RBP, QKI-5, which exerts anti-metastatic functions by destabilizing *TGF $\beta$ R1* mRNA and inactivating TGF- $\beta$ /SMAD signaling in LUADs. Of note, we established a novel mechanistic role of KLF6/QKI-5/TGF $\beta$ R1 axis controlling TGF- $\beta$ /SMAD signaling during TGF- $\beta$ -induced EMT and LUAD metastasis (Fig 7L).

Using a series of computational algorithms and tissue-based analyses, we verified that QKI is associated with tumor metastasis in LUAD because QKI expression was not only decreased in

unclassified LUAD tissues but reduced in metastatic LUAD tissues (Fig 1A and B). QKI has three major isoforms, including nuclear QKI-5 and cytoplasmic QKI-6/-7 (Wu *et al*, 1999). QKI-6 and QKI-7 were reported to be predominantly related to development and diseases of the nervous system (Ebersole *et al*, 1996; Larocque *et al*,

2009), while QKI-5 was widely studied in various human cancers including NSCLC (Zhou *et al*, 2017; Li *et al*, 2018; Kim *et al*, 2019). In the present study, we found that QKI-5 expression was far higher than QKI-6 and QKI-7 in LUAD cells (Fig 1H), suggesting that QKI-5 is a predominant isoform of QKI expressed in LUAD cells. Moreover,

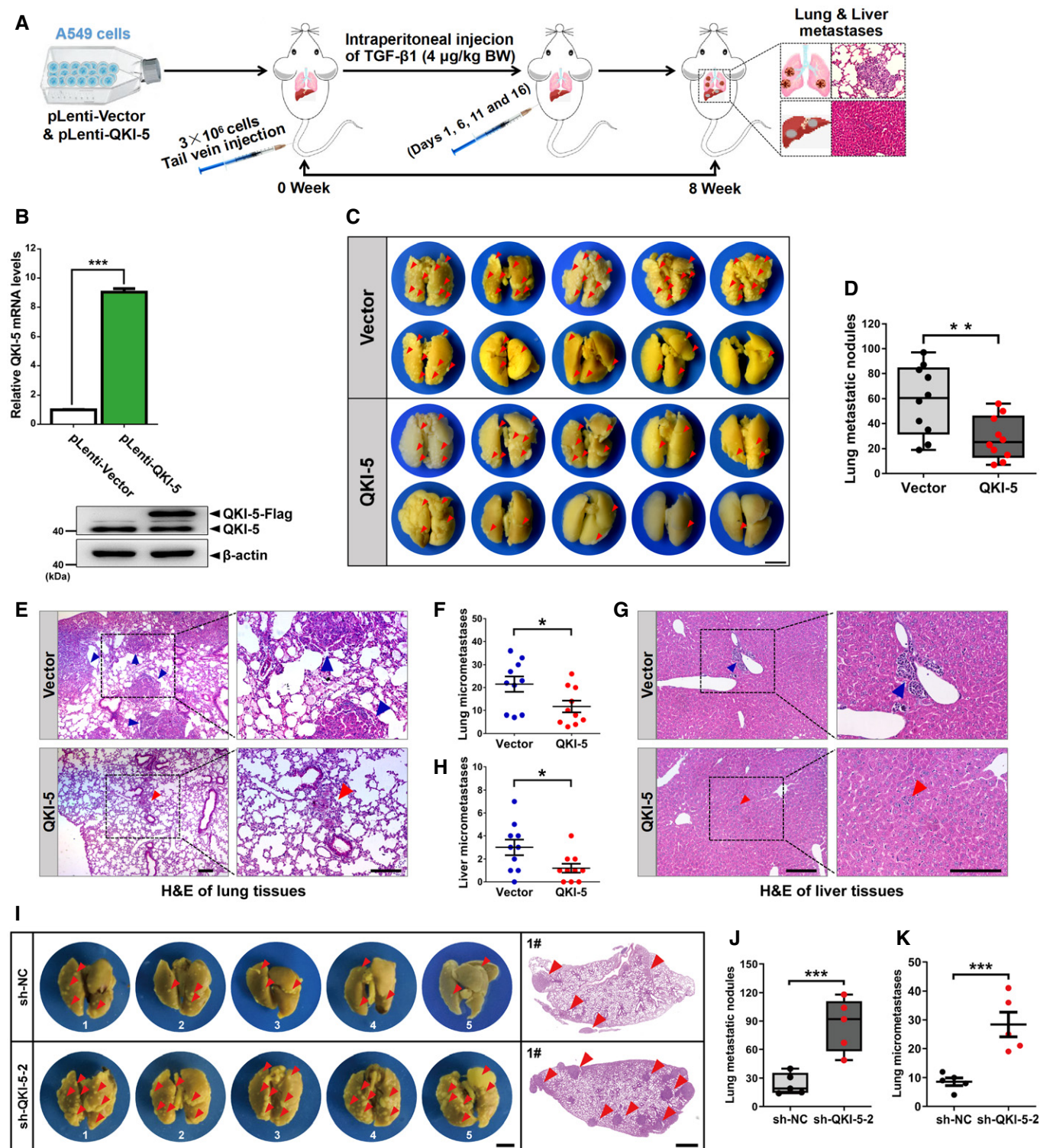


Figure 5.

**Figure 5. QKI-5 suppresses TGF- $\beta$ -stimulated LUAD cell metastasis *in vivo*.**

- A Schematic flowchart of LUAD cell *in vivo* metastasis model. QKI-5-overexpression and control vector A549 cells ( $3 \times 10^6$  cells/mouse) were i.v. injected into BALB/c nude mice (10 mice per group). TGF- $\beta$ 1 was injected i.p. at day 1, 6, 11, 16 after cell injection to achieve TGF- $\beta$ -stimulated A549 cell metastasis.
- B Before cell injection, QKI-5 was confirmed to overexpress in A549 cells using qRT-PCR and Western blot. Data are shown as the mean  $\pm$  SD of  $n = 3$  technical replicates. \*\*\* $P < 0.001$  by unpaired Student's *t*-test.
- C Representative images of lung metastatic nodules developed in mice 8 weeks after injection of QKI-5-overexpressing A549 cells or control A549 cells. The surgically resected lungs were stained as described in Materials and Methods. Red arrowheads indicate metastatic nodules established in lungs. Scale bar, 5 mm.
- D Comparison of the number of lung metastatic nodules between QKI-5-overexpressing group and vector group ( $n = 10$  mice per group). Data are shown as the boxplot. Central band: median; upper and lower line of boxes: upper and lower quartile; upper and lower line of whiskers: maximum and minimum. Data are shown as the mean  $\pm$  SEM. \*\* $P < 0.01$  by unpaired Student's *t*-test.
- E H&E staining was performed for the evaluation of lung micrometastases. Representative images showing micrometastases of lung tissues from a pair of mice referred in (C). Blue and red arrowheads indicate lung micrometastases of vector group and QKI-5-overexpressing group, respectively. Scale bar: 100  $\mu$ m.
- F Dot plots showing the difference of the micrometastases counts in lung tissues between QKI-5-overexpressing group and vector control group ( $n = 10$  mice per group). Data are shown as the mean  $\pm$  SEM. \* $P < 0.05$  by unpaired Student's *t*-test.
- G Representative microscopic photographs of H&E staining for liver micrometastases in a pair of mice referred in (E). Blue and red arrowheads indicate liver micrometastases. Scale bar: 100  $\mu$ m.
- H Dot plots showing the difference of the micrometastases counts in liver tissues between QKI-5-overexpressing group and control vector group ( $n = 10$  mice per group). Data are shown as the mean  $\pm$  SEM. \* $P < 0.05$  by unpaired Student's *t*-test.
- I Left part: Photographs of murine lungs with metastatic nodules after inoculation of sh-QKI-5-2 or sh-NC A549 cells. Scale bar, 5 mm. Right part: representative microscopic images of H&E staining for micrometastatic foci established in lungs from a pair of mice referred in left part. Scale bar, 1 mm. Red arrowheads indicate metastatic nodules and micrometastatic foci in lungs.
- J, K Dot plots showing the difference of the metastatic nodules (J) and micrometastases counts (K) in lung tissues between QKI-5-silenced group and control group ( $n = 5$  mice per group). In the boxplot, central band represents median, and upper and lower line of boxes represents upper and lower quartile, upper and lower line of whiskers represents maximum and minimum (J). Data are shown as the mean  $\pm$  SEM. \*\*\* $P < 0.001$  by unpaired Student's *t*-test.

Source data are available online for this figure.

low expression of QKI-5 was observed in LUAD cells and tissues, especially in metastatic LUAD tissues. Therefore, these findings promoted us to focus on QKI-5 and elucidate the mechanisms behind its metastasis-suppressive properties in LUADs. We have recently reported that TGF- $\beta$ -induced EMT plays an important role in LUAD cell metastasis (Wang *et al*, 2016; Wang *et al*, 2018; Tong *et al*, 2020). However, to the best of our knowledge, it has not been clear whether QKI-5 can affect TGF- $\beta$ -induced EMT during LUAD cell metastasis. Thus, we explored the involvement of QKI-5 in TGF- $\beta$ -induced EMT and its anti-metastatic potential in LUAD cells. Gain- and loss-of-function experiments showed that QKI-5 repressed TGF- $\beta$ -induced EMT and invasion of LUAD cells (Figs 4, 5, and EV1). In support of this, demonstrated that QKI-5 inhibited EMT and aggressiveness of LUAD cells; Kim and colleagues reported that knockdown of QKI induced EMT and enhanced cell invasion in oral squamous cell carcinoma (Kim *et al*, 2019).

QKIs perform diverse biological functions, such as regulation of RNA splicing and stability, or non-coding RNA processing (Zong *et al*, 2014; Conn *et al*, 2015; Zhou *et al*, 2017). In our study, QKI-5 can interact with *TGF $\beta$ 1* mRNA 3' UTR and decrease RNA stability of *TGF $\beta$ 1*, thereby deactivating TGF- $\beta$ /SMAD signaling (Figs 2 and 3). QKI isoforms including QKI-5 may interact with argonaute 2 (Ago2) (Wang *et al*, 2010). Ago2 is the core of the RNA-induced silencing complex (RISC) and may act as endonuclease activity in human cells, which mediates siRNA-triggered degradation of target mRNAs (Meister & Tuschl, 2004; Okamura *et al*, 2004). Thus, there would be the possibility that QKI-5 may destabilize *TGF $\beta$ 1* mRNA by interacting with and recruiting Ago2 to *TGF $\beta$ 1* 3'-UTR. Our investigation provided the first evidence for post-transcriptional repression of *TGF $\beta$ 1* by QKI-5. Recently, Zhou *et al* (2017) demonstrated that QKI-5 inhibits aggressiveness of LUAD cells through promoting  $\beta$ -catenin degradation. However, QKI-5 was reported to increased migration and invasion of breast cancer cells by modulating RNA splicing during EMT (Pillman *et al*, 2018). This discrepancy

is not surprising because QKI-5 may play distinct roles in cancer progression depending on cellular contexts.

In fact, TGF- $\beta$ /SMAD signaling acts as a metastasis promoter by inducing EMT in late-stage tumors (Akhurst & Derynck, 2001; Xu & Pasche, 2007; Chen *et al*, 2015). In this study, TGF $\beta$ 1, an essential receptor of TGF- $\beta$ /SMAD signaling, was found highly expressed in metastatic LUAD tissues. Moreover, TGF $\beta$ 1 knockdown significantly suppressed TGF- $\beta$ -induced EMT and metastasis of LUAD cells, which is supported by the finding that TGF $\beta$ 1 knockdown attenuated metastatic ability and enhanced chemosensitivity to cisplatin in LUAD cells (Wang *et al*, 2015). Therefore, TGF $\beta$ 1 knockdown showed similar effects as QKI-5 overexpression in LUAD cells (Fig EV2), thus functionally testing the mechanistic role of QKI-5 in *TGF $\beta$ 1* mRNA degradation. Furthermore, our rescue experiments demonstrated that QKI-5 inhibited TGF- $\beta$ -induced EMT and invasion of LUAD cells in a TGF $\beta$ 1-dependent manner (Figs 6 and EV3).

Why is *QKI-5* down-regulated in LUADs? Zhou *et al* (2017) found that *QKI-5* promoter hypermethylation caused a reduction of *QKI-5* expression in LUAD cells. This may be one of the underlying mechanisms responsible for the downregulation of the *QKI-5* gene. In fact, the mechanisms behind it should be more complicated. Thus, we tried to find specific transcriptional factors regulating the *QKI-5* gene and saw that KLF6 positively regulated *QKI-5* at the transcriptional level in LUAD cells. The functional KLF6-binding site we confirmed is localized at position +21 to +31 in the *QKI-5* gene (Fig 7G and H), which is different from the hypermethylation region (position -700 to +1) affecting *QKI-5* expression (Zhou *et al*, 2017). Besides, KLF6 was lowly expressed in LUAD tissues, especially in metastatic LUAD tissues (Appendix Tables S2 and S3), which is consistent with low expression of QKI-5. These data further suggested that *QKI-5* is a target of KLF6. However, we cannot exclude the possibility that there are other factors activating the transcription of *QKI-5*. For example, C/EBP can transcriptionally



activate *QKI-5* during macrophage differentiation (Fu *et al.*, 2012). Furthermore, our results showed that knockdown of *KLF6* increased *TGFβR1* expression and promoted TGF-β-induced EMT, which was partly abrogated by *QKI-5* overexpression in LUAD cells (Fig EV4). In contrast, in proximal tubule cells, *KLF6* not only promoted EMT induced by TGF-β1, but also *KLF6* expression was up-regulated by TGF-β1 (Holian *et al.*, 2008). Nevertheless, neither *KLF6* nor *QKI-5* expression were significantly affected by TGF-β1 in

LUAD cells (Fig EV5), implying that the regulation of *QKI-5* by *KLF6* is independent of TGF-β1.

Although *QKI-5* blocks TGF-β/SMAD signaling by degrading *TGFβR1* mRNA, it is possible that *QKI-5* regulates other TGF-β/SMAD signaling genes such as *BMPR2*, *MAPK1*, and *RHOA* (Fig 2B) via other mechanisms. In the present study, we have focused on *TGFβR1* because it is an indispensable upstream receptor in TGF-β/SMAD signaling. Further research is warranted to investigate other

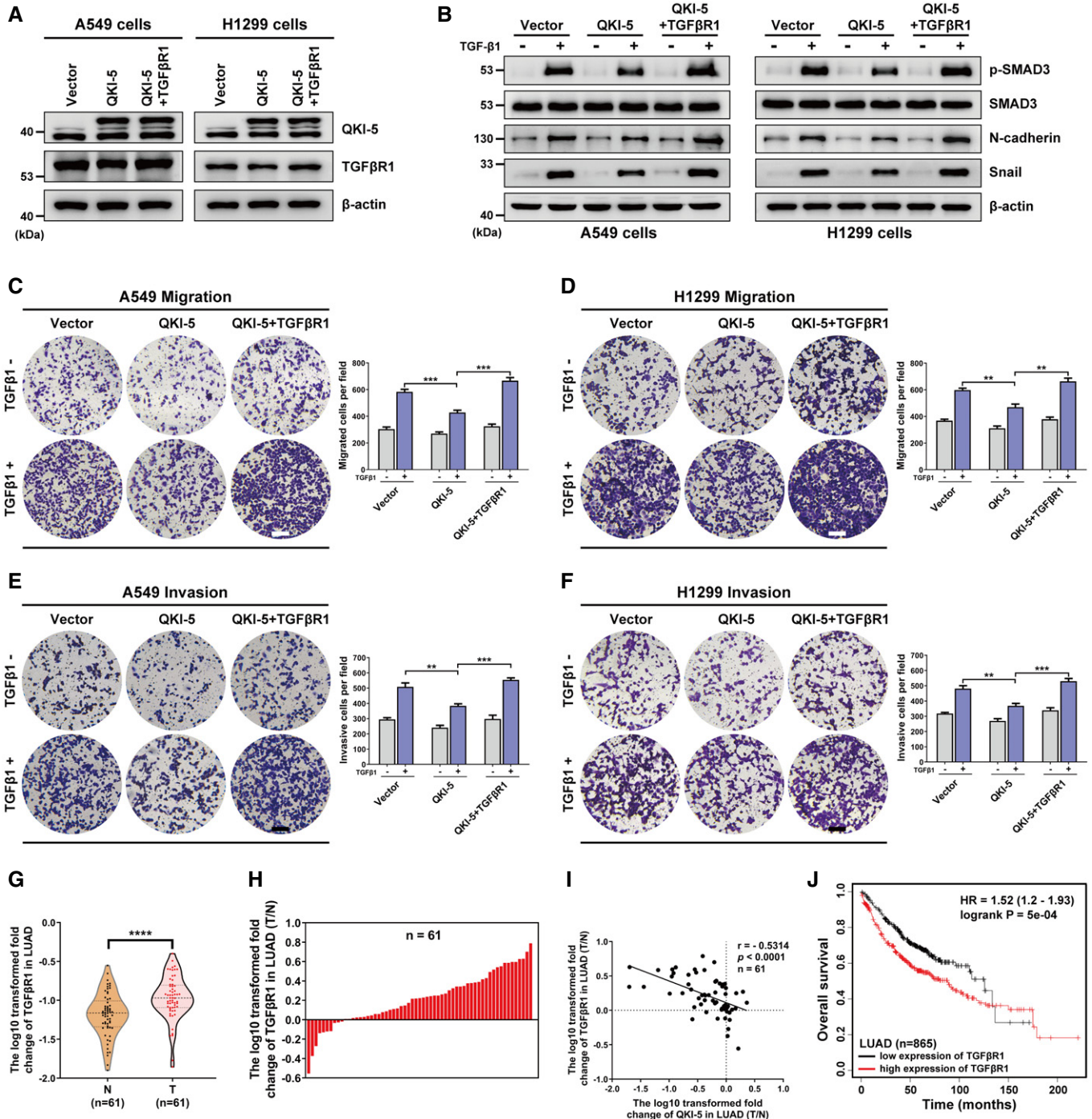


Figure 6.



**Figure 6. QKI-5 inhibits TGF- $\beta$ -induced EMT and cell invasion via a TGF $\beta$ R1-dependent manner.**

- A A549 and H1299 cells were co-transfected with QKI-5 and ORF-only of TGF $\beta$ R1 and then subjected to Western blot assays for detection of QKI-5 and TGF $\beta$ R1 expression.
- B After serum starvation for 24 h, the above-treated A549 and H1299 cells were stimulated with or without TGF- $\beta$ 1 (5 or 10 ng/ml) for 24 h. The expression of p-SMAD3, SMAD3, and EMT markers (N-cadherin and Snail) was determined using Western blot.  $\beta$ -actin was used as an internal control.
- C–F In the presence or absence of TGF- $\beta$ 1, the migratory and invasive capabilities of above-treated A549 and H1299 cells were evaluated by Transwell assays as described in Fig 4G–J. Migrated and invasive cells were stained and counted under a light microscope. Data are shown as the mean  $\pm$  SD of  $n = 3$  technical replicates.  $**P < 0.01$  and  $***P < 0.001$  by unpaired Student's  $t$ -test. Scale bar, 100  $\mu$ m.
- G, H qRT–PCR analysis of TGF $\beta$ R1 mRNA in 61 LUAD tissues and matched paracarcinoma tissues (G) and T/N mRNA expression of TGF $\beta$ R1 in 61 paired LUAD tissues (H). T, LUAD tissues; N, paracarcinoma tissues. Y axis represents the  $\log_{10}$ -transformed fold change of mRNA expression of TGF $\beta$ R1. Central dotted line of the violin plot represents median, and upper and lower dotted line represents quartile (G).  $****P < 0.0001$  by unpaired Student's  $t$ -test.
- I Correlation between QKI-5 and TGF $\beta$ R1 mRNA expression in 61 paired LUAD tissues. X and y axes represent the  $\log_{10}$ -transformed fold change of T/N expression ratios of QKI-5 and TGF $\beta$ R1 mRNA, respectively.  $P < 0.0001$  by Pearson's correlation test.
- J Kaplan–Meier survival curves (<http://kmpplot.com/analysis/>) of LUAD patients ( $n = 865$ ) with high or low expression levels of TGF $\beta$ R1. The log-rank test was used to compare the difference between two groups.

Source data are available online for this figure.

potential QKI-targeted genes and possible mechanisms. Moreover, a future challenge will be the evaluation of the function of the isoforms QKI-6/-7 in LUAD development and progression.

## Materials and Methods

### Cell lines and cell culture

Human lung adenocarcinoma (LUAD) cell lines A549 and H1299, immortalized human bronchial epithelial cell line BEAS-2B, and human embryonic kidney (HEK) 293T cells from the Cell Bank of Chinese Academy of Sciences were, respectively, cultured in RPMI 1640 medium (HyClone, South Logan, UT, USA) and Dulbecco's modified Eagle medium (DMEM; Thermo Fisher Scientific, Waltham, MA, USA) with 10% fetal bovine serum (FBS; Invitrogen, Carlsbad, CA, USA) at 37°C in a 5% CO<sub>2</sub> humidified incubator. A549 and H1299 cells were treated by TGF- $\beta$ 1 to elicit EMT following serum starvation for 24 h.

### Human LUAD tissue samples

Sixty-one fresh-frozen LUAD tissues and matched paracarcinoma tissues were obtained after informed consent from patients in the First Affiliated Hospital of Soochow University (Suzhou, China). LUAD patients were pathologically diagnosed and evaluated in accordance with the Revised International System for Staging Lung Cancer. The clinical characteristics of 61 LUAD patients are presented in Appendix Table S3, metastatic tissues ( $n = 28$ ) were from LUAD patients with local lymph node metastasis (T<sub>1–4</sub>N<sub>1–2</sub>M<sub>0</sub>) or distant organ metastasis (T<sub>1–4</sub>N<sub>any</sub>M<sub>1</sub>), and non-metastatic tissues ( $n = 33$ ) were from LUAD patients without any metastasis (T<sub>1–4</sub>N<sub>0</sub>M<sub>0</sub>). All of the LUAD patients enrolled in this study had not received either radiotherapy or chemotherapy before surgery. This work was authorized by the Ethics Committee of Soochow University.

### RNA extraction, qRT–PCR, and mRNA half-life assays

Total RNA isolation, cDNA synthesis, and qRT–PCR analysis were performed as previously described by us (Yang *et al*, 2015) with some modification. Expression of *ADARB1*, *CELF2*, *QKI*, *ZFP36*, *QKI-5/6/7*,

*TGF $\beta$ R1*, *E-cadherin*, *N-cadherin*, *PAI-1*, *Slug*, *Snail*, *KLF6*, etc., was normalized to  *$\beta$ -actin*. Relative mRNA levels were calculated using the  $\Delta\Delta C_t$  method. For mRNA half-life assay, 10  $\mu$ g/ml actinomycin D (Sigma-Aldrich, St. Louis, MO, USA) was added to A549 and H1299 cells. Total RNAs were extracted at the indicated time points for qRT–PCR assay. Primers used for qRT–PCR assay are listed in Appendix Table S5. Each RT–qPCR analysis was carried out three times.

### Western blot assay

Total protein was isolated from cell lysate and subjected to Western blot analysis according to our previous methods (Yang *et al*, 2015). The primary antibodies employed in Western blot were as follows: goat anti-TGF $\beta$ R1 (R&D Systems, Minneapolis, MN, USA), mouse anti-E-cadherin and anti-N-cadherin (BD Biosciences, San Jose, CA, USA), mouse anti-Snail, rabbit anti-SMAD3 and anti-p-SMAD3 and anti-Lamin B (Cell Signaling Technology, Danvers, MA, USA), rabbit anti-QKI (Abcam, Cambridge, MA, USA), rabbit anti-QKI-5 (Millipore, Billerica, MA, USA), mouse anti-KLF6 and anti- $\beta$ -actin, and anti-goat or anti-rabbit or anti-mouse secondary antibodies (Santa Cruz Biotechnology, Santa Cruz, CA, USA). The relative protein expression was normalized to  $\beta$ -actin. Each Western blot analysis was performed in triplicate, and representative bands were presented.

### Generation of LUAD cell lines stably overexpressing QKI-5

To generate A549 and H1299 cell lines stably overexpressing QKI-5, a  $\sim 1$ -kb coding sequence (GenBank Accession number: NM\_006775) of *QKI-5* was subcloned into a GV358 lentiviral expression vector (GeneChem Inc., Shanghai, China) containing a C-terminal 3 $\times$  Flag tag using endonucleases *AgeI/BamHI* (Fermentas, Glen Burnie, MD, USA). Primers used for amplifying the coding sequence of *QKI-5* were listed in Appendix Table S5. The empty lentivirus vector was served as a negative control. Subsequently, the QKI-5 expression construct or empty vector was co-transfected with packaging plasmids Helper 1.0 and Helper 2.0 (GeneChem Inc.) into HEK 293T cells using Lipofectamine 3000 (Invitrogen). At 48 h post-incubation in DMEM with 10% FBS, the packaged lentiviruses were collected and used to infect A549 and H1299 cells for 72 h. Finally, Flag-tagged QKI-5-overexpressing A549 and H1299 stable cells were selected with 2  $\mu$ g/ml puromycin (Solarbio Lifesciences, Beijing, China).

### Establishment of TGF $\beta$ 1-overexpressing LUAD cells

The coding sequence of *TGF $\beta$ 1* (GenBank Accession number: NM\_004612.4) was amplified with the corresponding primers (Forward: ACCTCCATAGAAGATTCTAGAATGGAGGCGGCGTCC CT; Reverse: AACATCGTATGGGTAGGATCCCATTTTGATGCCTTCC TGTGA) and subcloned into a pcDNA3.1 vector using endonucleases *Xba*I/*Bam*HI (New England Biolabs, Beverly, MA, USA) to generate pcDNA3.1-TGF $\beta$ 1 vectors. Then, A549 and H1299 cells were transiently transfected with above-constructed vectors using

Lipofectamine 3000 (Invitrogen). At 48 h post-transfection, the cells were harvested or treated for further experiments.

### Establishment of QKI-5-silenced and TGF $\beta$ 1-silenced stable LUAD cell lines

To establish QKI-5-silenced or TGF $\beta$ 1-silenced stable A549 and H1299 cell lines, the relative DNA fragments (sh-QKI-5-1, sh-QKI-5-2, sh-TGF $\beta$ 1-1, and sh-TGF $\beta$ 1-2; Appendix Table S6) were subcloned into a lentiviral vector pLKO.1-puro (GENEWIZ Inc., Suzhou, China)

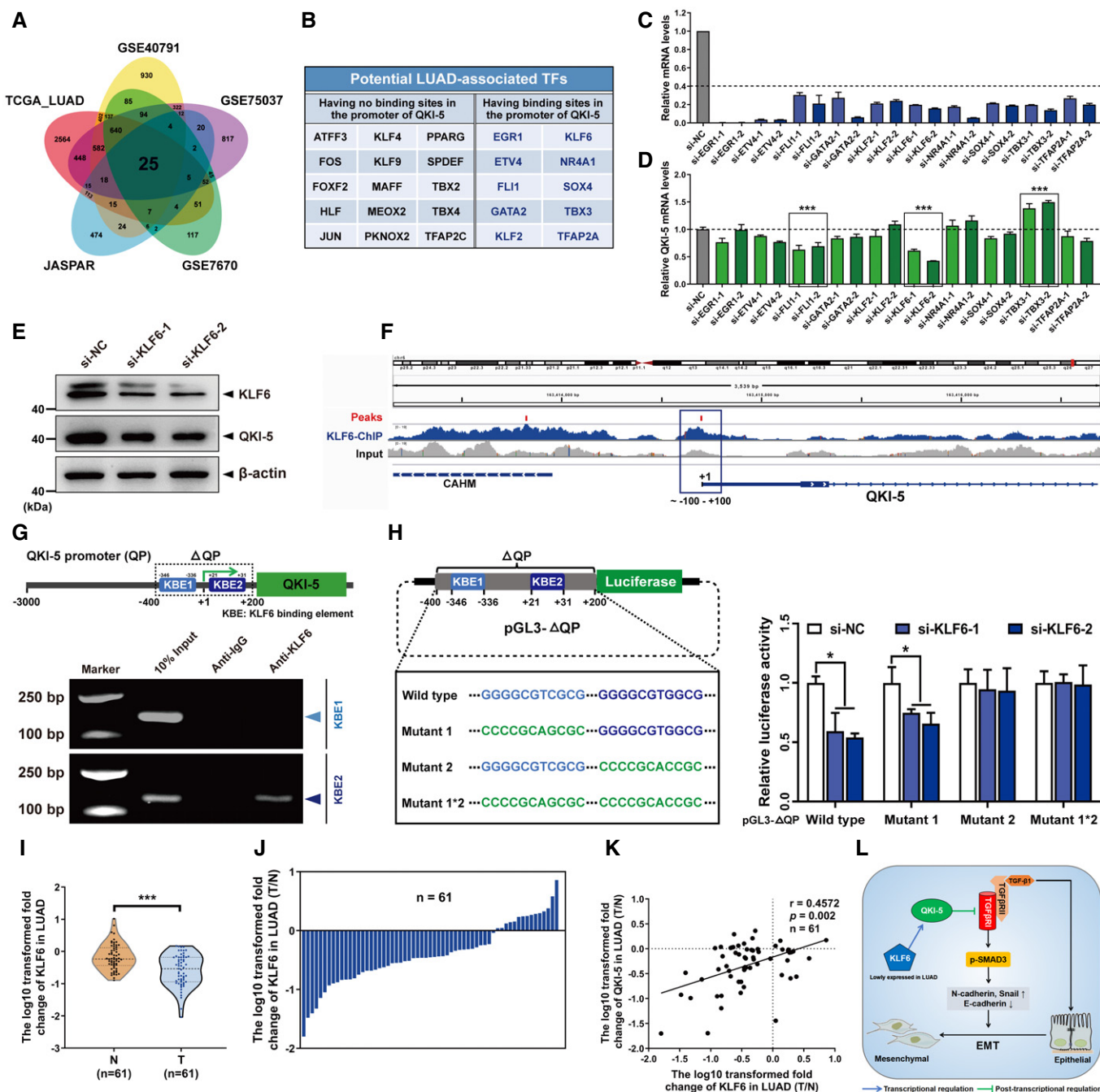


Figure 7.

**Figure 7. KLF6 transcriptionally regulates QKI-5 gene in LUADs.**

- A Four databases used in Fig 1A were intersected with human TFs database JASPAR to identify differentially expressed TFs in LUAD. The Venn diagram depicts the overlap between five independent data sets.
- B Listed are 25 LUAD-related differentially expressed TFs. TFBSTools was used to predict potential binding sites of each TF in *QKI-5* promoter sequence (position -3,000 to +200). TFBSTools minscore > 95%; TFs, transcription factors.
- C, D qRT-PCR analyses of mRNA expression of 10 TFs and *QKI-5* in A549 cells transfected with siRNAs of TFs, which have potential binding sites in *QKI-5* promoter. Data are shown as the mean  $\pm$  SD of  $n = 3$  technical replicates. \*\*\* $P < 0.001$  compared to si-NC by unpaired Student's *t*-test.
- E Western blot analysis of *QKI-5* protein levels in KLF6-silenced A549 cells.
- F An overview of KLF6-ChIP-seq data (GSE96355) is illustrated using Integrative Genomics Viewer (IGV) software. An obvious peak was detected at position -100 to +100 in the *QKI-5* promoter.
- G Upper panel: computational algorithms using PROMO and JASPAR predicted that two putative KBEs were harbored in  $\Delta$ QP region (position -400 to +200). QP, *QKI-5* promoter; KBE, KLF6 binding element. Lower panel: anti-KLF6 ChIP was conducted in A549 cells and followed by PCR and gel staining to confirm the presence of *QKI-5* promoter sequence containing KBE1 (position -346 to -336) or KBE2 (position +21 to +31). The input and anti-IgG antibody were used as positive and negative controls, respectively.
- H Left panel: Schematic drawing shows the pGL3- $\Delta$ QP luciferase reporter assay system. Boxed areas indicate four  $\Delta$ QP segments containing wild type or mutants of KBE1/2 (Mutant 1, Mutant 2, and Mutant 1\*2). Right panel: Four different pGL3- $\Delta$ QP luciferase reporter constructs were co-transfected with si-NC or si-KLF6 into A549 cells, and their luciferase activities were determined as described in Materials and Methods. Data are shown as the mean  $\pm$  SD of  $n = 3$  technical replicates. \* $P < 0.05$  compared to si-NC by unpaired Student's *t*-test.
- I, J qRT-PCR analysis of *KLF6* mRNA in 61 LUAD tissues and matched paracarcinoma tissues (I) and *T/N* mRNA expression of *KLF6* in 61 paired LUAD tissues (J). T, LUAD tissues; N, paracarcinoma tissues. Y axis represents the  $\log_{10}$ -transformed fold change of mRNA expression of *KLF6*. Central dotted line of the violin plot represents median, and upper and lower dotted line represents quartile (I). \*\*\* $P < 0.001$  by unpaired Student's *t*-test.
- K Correlation between *KLF6* and *QKI-5* mRNA expression in 61 paired LUAD tissues. X and y axes represent the  $\log_{10}$ -transformed fold change of T/N expression ratios of *KLF6* and *QKI-5* mRNA, respectively.  $P = 0.002$  by Pearson's correlation test.
- L A proposed work model: KLF6/*QKI-5*/TGF $\beta$ R1 axis regulates TGF- $\beta$ /SMAD signaling during TGF- $\beta$ -induced EMT.

Source data are available online for this figure.

with endonucleases *AgeI/EcoRI* (Fermentas). A scrambled sequence (sh-NC; Appendix Table S6) was used as a negative control. Then, the construct containing sh-*QKI-5* or sh-TGF $\beta$ R1 or sh-NC was co-transfected with packaging plasmids psPAX2 and pMD2.G into HEK 293T cells. The rest of the procedure is the same as that of generation of LUAD cell lines overexpressing *QKI-5* described above.

### RNA interference

Two short interfering RNAs (siRNAs) for each gene were designed and synthesized (GenePharma, Shanghai, China). A scrambled sequence was served as a negative control (si-NC). The sequences of synthesized siRNAs were listed in Appendix Table S6. A549 and H1299 cells were transiently transfected with 100 pmol of siRNAs using Lipofectamine 3000 (Invitrogen). At 72 h post-transfection, the cells were harvested or treated for further experiments.

### Luciferase reporter assay

To determine the effect of *QKI-5* on the luciferase activity of TGF $\beta$ R1 3' UTR, a series of constructs containing the wild-type and mutated (Mut) 3' UTR of TGF $\beta$ R1 fused to the 3'-end of the luciferase cDNA was generated using pGL3-Luc reporter vector (Promega, Madison, WI, USA). Briefly, different fragments (Appendix Table S4) were directly synthesized (GENEWIZ Inc.) and subcloned into pGL3-basic vector to create various constructs (pGL3-Luc-TGF $\beta$ R1 3' UTR wild type, pGL3-Luc-TGF $\beta$ R1 3' UTR-Mut1, pGL3-Luc-TGF $\beta$ R1 3' UTR-Mut2, and pGL3-Luc-TGF $\beta$ R1 3' UTR-Mut1\*2). Then, the above-mentioned constructs and pRL-TK plasmids were co-transfected into A549 and H1299 stable cell lines with vector or *QKI-5* overexpression using Lipofectamine 3000 (Invitrogen).

For analyzing transcriptional regulation of KLF6 on *QKI-5*, various *QKI-5* promoter fragments (Appendix Table S4) were synthesized and subcloned into pGL3-basic vector to generate the constructs

(pGL3-*QKI-5* promoter-wild-type-Luc, pGL3-*QKI-5* promoter-mutant 1-Luc, pGL3-*QKI-5* promoter-mutant 2-Luc, and pGL3-*QKI-5* promoter-mutant 1\*2-Luc). Subsequently, the above-mentioned constructs and pRL-TK plasmids were co-transfected into A549 and H1299 cells with si-NC or si-KLF6. At 48 h post-transfection, cells were harvested and luciferase activity was assessed using a Dual-Luciferase<sup>®</sup> Reporter Assay System (Promega). Results are presented as relative luciferase activities (firefly/*Renilla*), and each luciferase reporter analysis was performed in triplicate.

### In vitro RNA pull-down assay

The TGF $\beta$ R1 3' UTRs (Appendix Table S4) and an antisense sequence of TGF $\beta$ R1 3' UTR wild type were synthesized and labeled using biotin (RiboBio Biotech, Guangzhou, China). *In vitro* RNA pull-down assay was performed using Pierce<sup>™</sup> Magnetic RNA-Protein Pull-down Kit (Thermo Fisher Scientific) according to the manufacturer's protocol. Briefly, cell lysate was incubated with the beads containing biotin-labeled RNAs for 1 h at 4°C. After washing the beads, the bound proteins were eluted and boiled in 1  $\times$  SDS lysis buffer and subjected to Western blot analysis for determining the presence of *QKI-5*. Each experiment was done in triplicate.

### RNA-binding protein immunoprecipitation

RNA-binding protein immunoprecipitation (RIP) assay was conducted using EZ-Magna RIP Kit (Millipore) according to the manufacturer's protocol. The *QKI-5*-RIP experiments were performed in A549 and H1299 cells. Briefly, cells were lysed using RIP lysis buffer with protease inhibitor cocktail and RNase inhibitor (Millipore), and then, the RIP lysates were mixed with protein A/G magnetic beads incubated with rabbit anti-*QKI-5* antibody or anti-IgG antibody (Millipore) at 4°C overnight for immunoprecipitation. The rabbit IgG antibody was used as a negative control. The immunoprecipitated RNAs

were extracted and purified, and then subjected to RT-PCR and gel-staining analyses to determine the relative enrichment of interested mRNA immunoprecipitated by QKI-5 protein. Specific RIP primers used for PCR were summarized in Appendix Table S5.

### Chromatin immunoprecipitation

Chromatin immunoprecipitation (ChIP)-IT<sup>®</sup> Express Kit (Active Motif, Rixensart, Belgium) was used for ChIP analysis. The detailed protocol was performed as described earlier by us with modification (Tong *et al*, 2020). In this ChIP analysis, the chromatin fraction from cell nuclei was incubated with Protein G Agarose and anti-KLF6 antibody (Santa Cruz Biotechnology) overnight at 4°C. The ChIP-DNA was purified and used for PCR amplification with QKI-5-specific primers, which were provided in Appendix Table S5.

### Immunofluorescence (IF) analysis

Immunofluorescent analysis was performed as described by us (Wang *et al*, 2016) with somewhat modification. Briefly, cell samples were fixed with 4% paraformaldehyde and permeabilized with 0.5% Triton X-100 for 15 min and then blocked with 5% BSA for 1.5 h. Subsequently, cell samples were incubated with mouse anti-F-actin (Millipore) primary antibodies at 4°C overnight, followed by incubating with FITC-conjugated anti-mouse secondary antibody for 2.5 h. Cell nuclei were counterstained with 4',6-diamidino-2-phenylindole (DAPI). Finally, the cell samples were photographed using a LSM 700 confocal laser scanning microscope (Carl Zeiss, Jena, Germany), and representative images were presented.

### Wound-healing migration assay

A549 and H1299 cells were seeded and cultivated in six-well plates until they grew into a 90% confluent monolayer. Cells were then scratched by a sterilized pipette tip and cultured in serum-free medium with or without TGF- $\beta$ 1 (5 or 10 ng/ml) for 24 h. Cells were photographed in 6 random fields under a microscope. Cell migration distances into the scratched area were determined and analyzed using ImageJ Launcher software (National Institutes of Health, Bethesda, MA, USA). Each wound-healing analysis was repeated in triplicate.

### Transwell migration and invasion assays

Transwell migration and invasion assays were performed as described previously (Wang *et al*, 2016) with somewhat modification. Briefly,  $5 \times 10^4$  cells in 100  $\mu$ l RPMI 1640 medium with 1% FBS were added to the upper chamber of Transwell plates (BD Biosciences), and 700  $\mu$ l RPMI 1640 medium with 10% FBS was placed as a chemoattractant in the lower chamber. After 6 h, TGF- $\beta$ 1 (5 or 10 ng/ml) was added to the lower chambers. After incubation for 24 h (migration) or 30 h (invasion) in 37°C, the inserts were removed and the non-migrating or non-invading cells were removed with cotton swabs. Cells that migrated or invaded to the lower chamber were fixed and stained with 1% crystal violet. Cells were photographed and counted in at least four random fields. Each Transwell migration and invasion analysis was performed in triplicate.

### In vivo metastasis assays

Four-week-old female BALB/c nude mice were purchased from Laboratory Animal Center of Soochow University and housed under specific pathogen-free conditions. The mice were divided into four groups, including control vector groups and QKI-5 overexpression group, control sh-NC group and sh-QKI-5 group (10 or 5 mice per group). QKI-5-overexpressing, QKI-5-silenced, and control A549 cells ( $3 \times 10^6$  cells/mouse) in 200- $\mu$ l of PBS were intravenously (i.v.) injected into the tail vein of mice. At every 5<sup>th</sup> day post-inoculation, TGF- $\beta$ 1 (4  $\mu$ g/kg bodyweight) was intraperitoneally (i.p.) injected as previously described (Wang *et al*, 2018) to promote tumor cell metastasis. Eight weeks later, the mice were euthanized; then their lungs and livers were taken out and fixed in Bouin's solution for macroscopically metastatic nodule analysis. Lung and liver tissues were histologically examined by hematoxylin-eosin (H&E) staining for tumor cell micrometastases analysis. Animal studies were approved and supervised by the Animal Ethics Committee of Soochow University.

### Statistical analysis

Unpaired *t*-test (two-tailed) was used to assess comparisons between two groups *in vitro* data, *in vivo* data, and LUAD sample data. Differences between multiple groups in the clinicopathological character of LUAD were assessed by non-parametric tests (Unpaired *t*-test for two groups, and Kruskal–Wallis test for  $\geq 3$  groups). The association between two groups of LUAD sample data was analyzed by Pearson's correlation test. Data were expressed as mean  $\pm$  SD/SEM. *P* values of  $< 0.05$  were considered to be statistically significant. GraphPad Prism 7.01 (GraphPad, San Diego, CA, USA) was used for all statistical analyses.

### Bioinformatic analysis of public data sets

TCGA\_LUAD data set from Genomic Data Commons (GDC) database (<https://gdc.cancer.gov/>) and data sets including GSE40791, GSE75037, and GSE7670 from Gene Expression Omnibus (GEO) database (<https://www.ncbi.nlm.nih.gov/geo/>) are downloaded to screen for LUAD-associated RBPs and TFs. Differentially expressed genes (DEGs) are statistically considered as significance with FDR  $< 0.01$  and  $\text{abs.log}_2\text{FC} > 1$  in TCGA database, and adjusted *P*-value  $< 0.01$  and  $\text{abs.log}_2\text{FC} > 1$  in GEO database. The DEGs of the above-mentioned four data sets are intersected with human RBPs database ATTRACT (Giudice *et al*, 2016) or with TFs database JASPAR (Fornes *et al*, 2020) to yield LUAD-associated RBPs or TFs. TFBSTools is conducted to predict potential binding sites of each LUAD-associated TFs in QKI-5 promoter sequence (position  $-3,000$  to  $+200$ ). TFBSTools minscore  $> 95\%$  is applied as selection criteria.

Kaplan–Meier Plotter (<http://www.kmplot.com>) database and log-rank tests are performed to evaluate the prognostic value of QKI (data from 236154\_at) and TGF $\beta$ R1 (data from TCGA) in lung cancer patients.

Three QKI-RIP-seq data from POSTAR, EuRBPDB, and doRiNA databases (Blin *et al*, 2015; Zhu *et al*, 2019; Liao *et al*, 2020) are overlapped to identify potential QKI-targeted genes. Subsequently, KEGG enrichment analysis of these potential QKI-targeted genes is performed by clusterProfiler in R language. A conserved consensus



QKI-5 response element (QRE) is computationally generated using RBPmap database (<http://rbpmap.technion.ac.il/index.html>).

For ChIP-seq data analysis, KLF6-ChIP-seq reads from GEO database (GSE96355) are aligned to human genome reference (hg38) using Bowtie2 with default parameters. The mapping reads from ChIP-seq are preprocessed by Samtools and then submitted to MACS2 for peaks calling. The characterized peaks are annotated by the R package ChIPseeker and visualized with Integrative Genomics Viewer (IGV) software.

## Data availability

No primary data sets have been generated and deposited.

**Expanded View** for this article is available online.

## Acknowledgements

We are grateful for participation and cooperation from LUAD patients. Funding was provided by grants from National Natural Science Foundation of China (81872343, 81672277), and Suzhou Key Laboratory for Molecular Cancer Genetics (SZS201209), and A Project Funded by the Priority Academic Program Development of Jiangsu Higher Education Institutions (PAPD).

## Author contributions

Conception and design: SW and H-TZ; Development of methodology: SW, XT, and CL; Acquisition of data (provided animals, acquired and managed patients, provided facilities, etc.): SW, XT, CL, EJ, ZhS, ZeS, WZ, and ZL; Analysis and interpretation of data (e.g., statistical analysis, biostatistics, computational analysis): SW, XT, and CL; Writing, review, and/or revision of the manuscript: SW and H-TZ. Administrative, technical, or material support (i.e., reporting or organizing data, constructing databases): SW, XT, and CL. Study supervision: H-TZ.

## Conflict of interest

The authors declare that they have no conflict of interest.

## References

- Akhurst RJ, Derynck R (2001) TGF-beta signaling in cancer—a double-edged sword. *Trends Cell Biol* 11: S44–S51
- Blin K, Dieterich C, Wurmus R, Rajewsky N, Landthaler M, Akalin A (2015) DoRiNA 2.0—upgrading the doRiNA database of RNA interactions in post-transcriptional regulation. *Nucleic Acids Res* 43: D160–D167
- Chen CH, Lai JM, Chou TY, Chen CY, Su LJ, Lee YC, Cheng TS, Hong YR, Chou CK, Whang-Peng J et al (2009) VEGFA upregulates FLJ10540 and modulates migration and invasion of lung cancer via PI3K/AKT pathway. *PLoS One* 4: e5052
- Chen Z, Fillmore CM, Hammerman PS, Kim CF, Wong KK (2014) Non-small-cell lung cancers: a heterogeneous set of diseases. *Nat Rev Cancer* 14: 535–546
- Chen H, Yang T, Lei Z, Wang L, Yang H, Tong X, Yang WT, Zhao J, Gu Y, Chen Y et al (2015) RNF111/Arkadia is regulated by DNA methylation and affects TGF-beta/Smad signaling associated invasion in NSCLC cells. *Lung Cancer* 90: 32–40
- Conn SJ, Pillman KA, Toubia J, Conn VM, Salmanidis M, Phillips CA, Roslan S, Schreiber AW, Gregory PA, Goodall GJ (2015) The RNA binding protein quaking regulates formation of circRNAs. *Cell* 160: 1125–1134
- ten Dijke P, Hill CS (2004) New insights into TGF-beta-Smad signalling. *Trends Biochem Sci* 29: 265–273
- Dongre A, Weinberg RA (2019) New insights into the mechanisms of epithelial-mesenchymal transition and implications for cancer. *Nat Rev Mol Cell Biol* 20: 69–84
- Du B, Shim JS (2016) Targeting epithelial-mesenchymal transition (EMT) to overcome drug resistance in cancer. *Molecules* 21: 965
- Ebersole TA, Chen Q, Justice MJ, Artzt K (1996) The quaking gene product necessary in embryogenesis and myelination combines features of RNA binding and signal transduction proteins. *Nat Genet* 12: 260–265
- Fang Y, Chen Y, Yu L, Zheng C, Qi Y, Li Z, Yang Z, Zhang Y, Shi T, Luo J et al (2013) Inhibition of breast cancer metastases by a novel inhibitor of TGFbeta receptor 1. *J Natl Cancer Inst* 105: 47–58
- Fornes O, Castro-Mondragon JA, Khan A, van der Lee R, Zhang X, Richmond PA, Modi BP, Corread S, Gheorghe M, Baranasic D et al (2020) JASPAR 2020: update of the open-access database of transcription factor binding profiles. *Nucleic Acids Res* 48: D87–D92
- Fu H, Yang G, Wei M, Liu L, Jin L, Lu X, Wang L, Shen L, Zhang J, Lu H et al (2012) The RNA-binding protein QKI5 is a direct target of C/EBPalpha and delays macrophage differentiation. *Mol Biol Cell* 23: 1628–1635
- Galarneau A, Richard S (2005) Target RNA motif and target mRNAs of the Quaking STAR protein. *Nat Struct Mol Biol* 12: 691–698
- Girard L, Rodriguez-Canales J, Behrens C, Thompson DM, Botros IW, Tang H, Xie Y, Rektman N, Travis WD, Wistuba II et al (2016) An expression signature as an aid to the histologic classification of non-small cell lung cancer. *Clin Cancer Res* 22: 4880–4889
- Giudice G, Sanchez-Cabo F, Torroja C, Lara-Pezzi E (2016) ATRACT—a database of RNA-binding proteins and associated motifs. *Database (Oxford)* 2016: baw035
- Holian J, Qi W, Kelly DJ, Zhang Y, Mreich E, Pollock CA, Chen XM (2008) Role of Kruppel-like factor 6 in transforming growth factor-beta1-induced epithelial-mesenchymal transition of proximal tubule cells. *Am J Physiol Renal Physiol* 295: F1388–F1396
- Ito G, Uchiyama M, Kondo M, Mori S, Usami N, Maeda O, Kawabe T, Hasegawa Y, Shimokata K, Sekido Y (2004) Kruppel-like factor 6 is frequently down-regulated and induces apoptosis in non-small cell lung cancer cells. *Cancer Res* 64: 3838–3843
- Jett JR, Cortese DA, Fontana RS (1983) Lung cancer: current concepts and prospects. *CA Cancer J Clin* 33: 74–86
- Kim EJ, Kim JS, Lee S, Lee H, Yoon JS, Hong JH, Chun SH, Sun S, Won HS, Hong SA et al (2019) QKI, a miR-200 target gene, suppresses epithelial-to-mesenchymal transition and tumor growth. *Int J Cancer* 145: 1585–1595
- Kudinov AE, Deneka A, Nikonova AS, Beck TN, Ahn YH, Liu X, Martinez CF, Schultz FA, Reynolds S, Yang DH et al (2016) Musashi-2 (MSI2) supports TGF-beta signaling and inhibits claudins to promote non-small cell lung cancer (NSCLC) metastasis. *Proc Natl Acad Sci USA* 113: 6955–6960
- Kuhn E, Morbini P, Cancellieri A, Damiani S, Cavazza A, Comin CE (2018) Adenocarcinoma classification: patterns and prognosis. *Pathologica* 110: 5–11
- Lamouille S, Xu J, Derynck R (2014) Molecular mechanisms of epithelial-mesenchymal transition. *Nat Rev Mol Cell Biol* 15: 178–196
- Larocque D, Pilotte J, Chen T, Cloutier F, Massie B, Pedraza L, Couture R, Lasko P, Almazan G, Richard S (2002) Nuclear retention of MBP mRNAs in the quaking viable mice. *Neuron* 36: 815–829
- Larocque D, Fragoso G, Huang J, Mushynski WE, Loignon M, Richard S, Almazan G (2009) The QKI-6 and QKI-7 RNA binding proteins block proliferation and promote Schwann cell myelination. *PLoS One* 4: e5867

- Li J, Choi PS, Chaffer CL, Labelle K, Hwang JH, Giacomelli AO, Kim JW, Ilic N, Doench JG, Ly SH et al (2018) An alternative splicing switch in FLNB promotes the mesenchymal cell state in human breast cancer. *Elife* 7
- Liang G, Meng W, Huang X, Zhu W, Yin C, Wang C, Fassan M, Yu Y, Kudo M, Xiao S et al (2020) miR-196b-5p-mediated downregulation of TSPAN12 and GATA6 promotes tumor progression in non-small cell lung cancer. *Proc Natl Acad Sci USA* 117: 4347–4357
- Liao JY, Yang B, Zhang YC, Wang XJ, Ye Y, Peng JW, Yang ZZ, He JH, Zhang Y, Hu K et al (2020) EuRBPDB: a comprehensive resource for annotation, functional and oncological investigation of eukaryotic RNA binding proteins (RBPs). *Nucleic Acids Res* 48: D307–D313
- Meister G, Tuschl T (2004) Mechanisms of gene silencing by double-stranded RNA. *Nature* 431: 343–349
- Mikami F, Lim JH, Ishinaga H, Ha UH, Gu H, Koga T, Jono H, Kai H, Li JD (2006) The transforming growth factor-beta-Smad3/4 signaling pathway acts as a positive regulator for TLR2 induction by bacteria via a dual mechanism involving functional cooperation with NF-kappaB and MAPK phosphatase 1-dependent negative cross-talk with p38 MAPK. *J Biol Chem* 281: 22397–22408
- Muppala S, Xiao R, Krukovets I, Verbovetsky D, Yendamuri R, Habib N, Raman P, Plow E, Stenina-Adognravi O (2017) Thrombospondin-4 mediates TGF-beta-induced angiogenesis. *Oncogene* 36: 5189–5198
- Narla G, Heath KE, Reeves HL, Li D, Giono LE, Kimmelman AC, Glucksmann MJ, Narla J, Eng FJ, Chan AM et al (2001) KLF6, a candidate tumor suppressor gene mutated in prostate cancer. *Science* 294: 2563–2566
- Okamura K, Ishizuka A, Siomi H, Siomi MC (2004) Distinct roles for Argonaute proteins in small RNA-directed RNA cleavage pathways. *Genes Dev* 18: 1655–1666
- Pastushenko I, Blanpain C (2019) EMT transition states during tumor progression and metastasis. *Trends Cell Biol* 29: 212–226
- Pillman KA, Phillips CA, Roslan S, Toubia J, Dredge BK, Bert AG, Lumb R, Neumann DP, Li X, Conn SJ et al (2018) miR-200/375 control epithelial plasticity-associated alternative splicing by repressing the RNA-binding protein Quaking. *EMBO J* 37: e99016
- Reeves HL, Narla G, Ogunbiyi O, Haq AI, Katz A, Benzeno S, Hod E, Harpaz N, Goldberg S, Tal-Kremer S et al (2004) Kruppel-like factor 6 (KLF6) is a tumor-suppressor gene frequently inactivated in colorectal cancer. *Gastroenterology* 126: 1090–1103
- Rodrigues DC, Kim DS, Yang G, Zaslavsky K, Ha KC, Mok RS, Ross PJ, Zhao M, Piekna A, Wei W et al (2016) MECP2 is post-transcriptionally regulated during human neurodevelopment by combinatorial action of RNA-binding proteins and miRNAs. *Cell Rep* 17: 720–734
- Saccomanno L, Loushin C, Jan E, Punkay E, Artzt K, Goodwin EB (1999) The STAR protein QKI-6 is a translational repressor. *Proc Natl Acad Sci USA* 96: 12605–12610
- Schmierer B, Hill CS (2007) TGFbeta-SMAD signal transduction: molecular specificity and functional flexibility. *Nat Rev Mol Cell Biol* 8: 970–982
- Siegel RL, Miller KD, Jemal A (2019) Cancer statistics, 2019. *CA Cancer J Clin* 69: 7–34
- Thangaraj MP, Furber KL, Gan JK, Ji S, Sobchishin L, Doucette JR, Nazarali AJ (2017) RNA-binding protein quaking stabilizes Sirt2 mRNA during oligodendroglial differentiation. *J Biol Chem* 292: 5166–5182
- Tong X, Wang S, Lei Z, Li C, Zhang C, Su Z, Liu X, Zhao J, Zhang HT (2020) MYOCD and SMAD3/SMAD4 form a positive feedback loop and drive TGF-beta-induced epithelial-mesenchymal transition in non-small cell lung cancer. *Oncogene* 39: 2890–2904
- Wang Y, Lacroix G, Haines J, Doukhanine E, Almazan G, Richard S (2010) The QKI-6 RNA binding protein localizes with the MBP mRNAs in stress granules of glial cells. *PLoS One* 5: e12824
- Wang Y, Vogel G, Yu Z, Richard S (2013) The QKI-5 and QKI-6 RNA binding proteins regulate the expression of microRNA 7 in glial cells. *Mol Cell Biol* 33: 1233–1243
- Wang X, Chen X, Meng Q, Jing H, Lu H, Yang Y, Cai L, Zhao Y (2015) MiR-181b regulates cisplatin chemosensitivity and metastasis by targeting TGFbetaR1/Smad signaling pathway in NSCLC. *Sci Rep* 5: 17618
- Wang L, Yang H, Lei Z, Zhao J, Chen Y, Chen P, Li C, Zeng Y, Liu Z, Liu X et al (2016) Repression of TIF1gamma by SOX2 promotes TGF-beta-induced epithelial-mesenchymal transition in non-small-cell lung cancer. *Oncogene* 35: 867–877
- Wang L, Tong X, Zhou Z, Wang S, Lei Z, Zhang T, Liu Z, Zeng Y, Li C, Zhao J et al (2018) Circular RNA hsa\_circ\_0008305 (circPTK2) inhibits TGF-beta-induced epithelial-mesenchymal transition and metastasis by controlling TIF1gamma in non-small cell lung cancer. *Mol Cancer* 17: 140
- Wu J, Zhou L, Tonissen K, Tee R, Artzt K (1999) The quaking I-5 protein (QKI-5) has a novel nuclear localization signal and shuttles between the nucleus and the cytoplasm. *J Biol Chem* 274: 29202–29210
- Xu Y, Pasche B (2007) TGF-beta signaling alterations and susceptibility to colorectal cancer. *Hum Mol Genet* 16: R14–R20
- Yang H, Wang L, Zhao J, Chen Y, Lei Z, Liu X, Xia W, Guo L, Zhang HT (2015) TGF-beta-activated SMAD3/4 complex transcriptionally upregulates N-cadherin expression in non-small cell lung cancer. *Lung Cancer* 87: 249–257
- Zhang Y, Foreman O, Wigle DA, Kosari F, Vasmatzis G, Salisbury JL, van Deursen J, Galardy PJ (2012) USP44 regulates centrosome positioning to prevent aneuploidy and suppress tumorigenesis. *J Clin Invest* 122: 4362–4374
- Zhou X, Li X, Sun C, Shi C, Hua D, Yu L, Wen Y, Hua F, Wang Q, Zhou Q et al (2017) Quaking-5 suppresses aggressiveness of lung cancer cells through inhibiting beta-catenin signaling pathway. *Oncotarget* 8: 82174–82184
- Zhu Y, Xu G, Yang YT, Xu Z, Chen X, Shi B, Xie D, Lu ZJ, Wang P (2019) POSTAR2: deciphering the post-transcriptional regulatory logics. *Nucleic Acids Res* 47: D203–D211
- Zong FY, Fu X, Wei WJ, Luo YG, Heiner M, Cao LJ, Fang Z, Fang R, Lu D, Ji H et al (2014) The RNA-binding protein QKI suppresses cancer-associated aberrant splicing. *PLoS Genet* 10: e1004289



**License:** This is an open access article under the terms of the Creative Commons Attribution-NonCommercial-NoDerivs License, which permits use and distribution in any medium, provided the original work is properly cited, the use is non-commercial and no modifications or adaptations are made.